united nations
national, scientific
and cultural
organization

international atomic
energy agency

the
abdus salam
international centre for theoretical physics

SMR.1135 - 11

THIRD WORKSHOP ON
THIN FILMS PHYSICS AND TECHNOLOGY
(8 - 24 MARCH 1999)
including
TOPICAL CONFERENCE ON
MICROSTRUCTURE AND SURFACE MORPHOLOGY
EVOLUTION IN THIN FILMS
(24 - 26 MARCH 1999)

"Thermodynamics and kinetics of nucleation and the early stages of film growth"

Joseph GREENE
University of Illinois at Urbana-Champaign
Frederic Seitz Materials Research Laboratory
104 South Goodwin Avenue
61801-2985 Urbana
U.S.A.

3rd ICTP/IUVSTA Workshop on Thin Film Physics
Trieste, Italy

Thermodynamics and Kinetics of Nucleation And the Early Stages of Film Growth

Joe Greene
University of Illinois

Monday, March 22, 14:00 to 16:00

Outline:

1. Introduction: surface structure and processes
2. Nucleation
    a. Thermodynamics
    b. Kinetics
3. 2-D nucleation and growth
    a. Step flow
        1. Mechanisms and kinetics
        2. Transition to layer-by-layer
    b. Layer-by-layer
        1. Mechanisms and kinetics
        2. Fundamental limits
        3. Transition to multilayer growth
    c. Multilayer growth
        1. Kinetic roughening, critical thickness
            * Surfactants
            * Energetic condensing species

Thin Film Nucleation

Prof. J.E. Greene
University of Illinois

General References:

1. J.P. Hirth and G.M. Pound, *Condensation and Evaporation: Nucleation and Growth Kinetics*, MacMillan Co., New York (1963).
2. G.M. Pound and J.P. Hirth, "Heterogeneous Nucleation on Substrates," in *Condensation and Evaporation of Solids*, ed. by E. Rutner, P. Goldfinger, and J.P. Hirth, Gordon and Breach, New York (1964).
3. T.N. Rhodin, "Nucleation and Growth on Solid Surfaces: Theory and Applications," in *The Use of Thin Films in Physics Investigations*, ed. by J.C. Anderson, Academic Press, New York (1966).
4. C.A. Neugebaur, "Condensation, Nucleation and Growth of Thin Films," in *Handbook of Thin Film Technology*," ed. by L.I. Maissel and R. Glang, McGraw-Hill, New York (1970).
5. J.A. Venables and G.L. Price, "Nucleation of Thin Films," in *Epitaxial Growth*, Part B, ed. by J.W. Matthews, Academic Press, New York (1975).
6. B. Lewis, "Nucleation and Growth Theory," in *Crystal Growth*, ed. by B.R. Pamplin, Pergamon Press, New York (1975).
7. R.J.H. Voorhoeve, "Molecular Beam Deposition of Solids on Surfaces: Ultrathin Films," in Treatise on Solid State Chemistry, Vol. 6A, Surfaces I, ed. by N.B. Hannay, Plenum Press, New York (1976).
8. J.A. Venables, G.D.T. Spiller, and M. Hanbücken, "Nucleation and Growth of Thin Films," *Rep. Prog. Phys. 47*, 399 (1984).
9. A. Zangwill, *Physics at Surfaces*, Cambridge University press, Cambridge, UK, 1988,
10. K.N. Tu, J.W. Mayer, and L.C. Feldman, *Electronic Thin Film Science*, Macmillian, New York (1992).
11. J.E. Greene, "The Role of Low-Energy Ion/Surface Interaction Effects During Crystal Growth from the Vapor Phase: Nucleation and Growth, Microstructure Evolution, and Defect Formation and Annihilation," in *Handbook of Crystal Growth, Volume 1: Fundamentals*, ed. by D.T.J. Hurle, Elsevier, Amsterdam, The Netherlands (1993), p. 639.
12. J.E. Greene, "Physics of Film Growth from the Vapor Phase," in *Multicomponent and Multilayered Thin Films for Advanced Technologies: Techniques, Fundamentals, and Devices*, ed. by O. Auciello, NATO Advanced Study Institute, Kluwer Academic Publishers Boston (1993), p. 39.
13. J.T. Tsao, *Materials Fundamentals of MBE*, Academic Press, Boston, MA (1993).

Kinetics of Surface Processes: an Introduction

Surface = planar defect in a crystalline solid; an interruption in a periodic array of atoms; an interface between solid and vapor phases.

E_s = surface site energy
ΔH_s = enthalpy of sublimation

Crystal	T (K)	E_s (eV/site)*	ΔH_s (eV/site)
W (001)	2000	2.3	8.7
Nb (001)	2523	2.1	7.7
Pt (110)	1583	1.9	5.9
Au (110)	1300	1.5	3.7
Ag (110)	1180	1.3	3.0
Cu (110)	1320	1.4	3.6
Si (111)	77	1.0	4.6
Ge (111)	77	0.9	3.9

(G. Ehrlich, Br. J. Appl. Phys. 15, 349 (1964)).

Note that $E_s \approx (1/3 \text{ to } 1/4)\, \Delta H_s$

* 1 eV/particle ≡ 23.06 kcal/mole

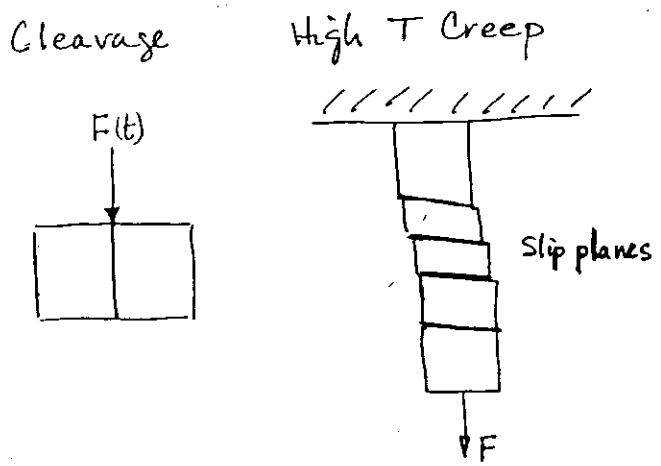

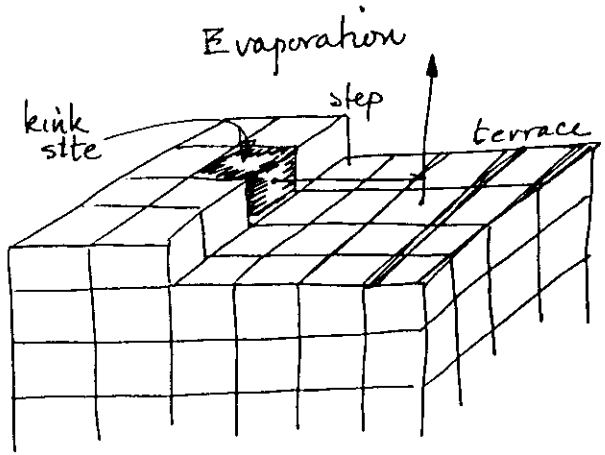

Surface sites ≡ regions of high free energy associated with highly reactive unsatisfied bonds.

M. Kitabatake, P. Fons, J.E. Greene
J. Vac. Sci. Technol. A8, 3726 (1990).

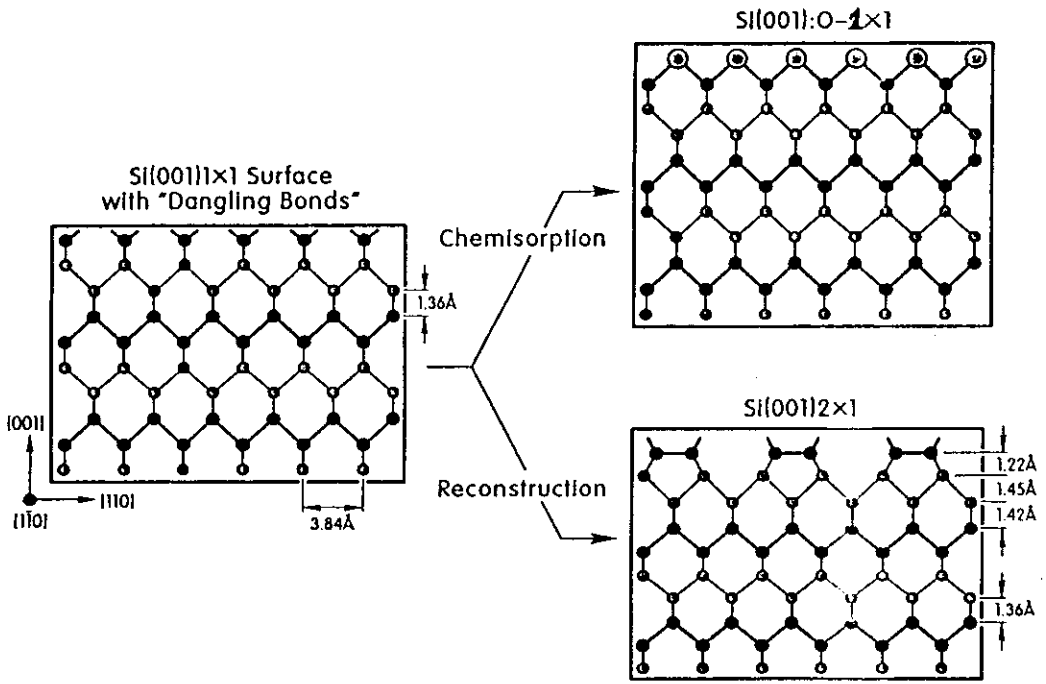

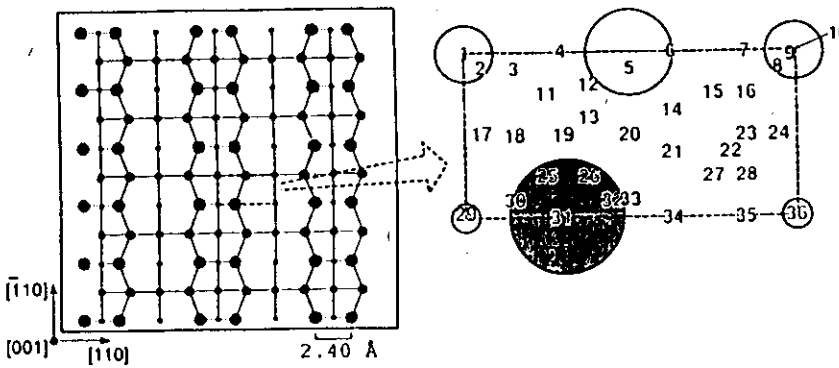

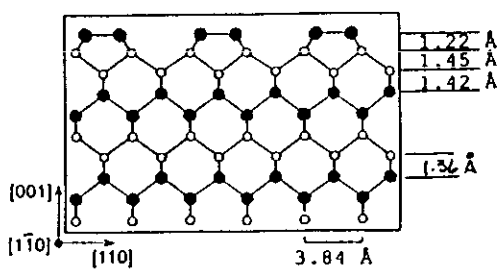

- 1st layer atom
- 2nd layer atom
- 3rd layer atom
- 4th layer atom

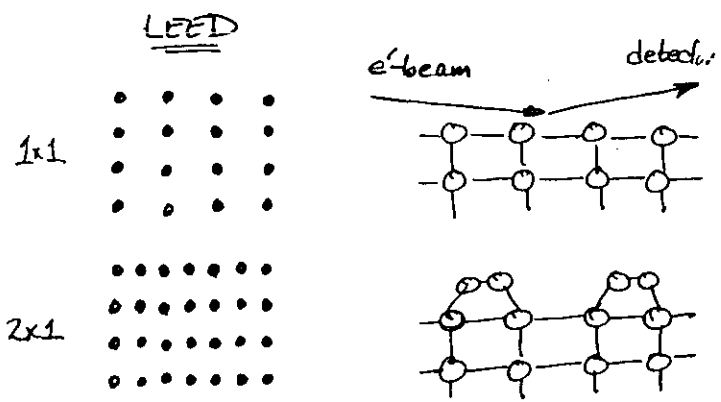

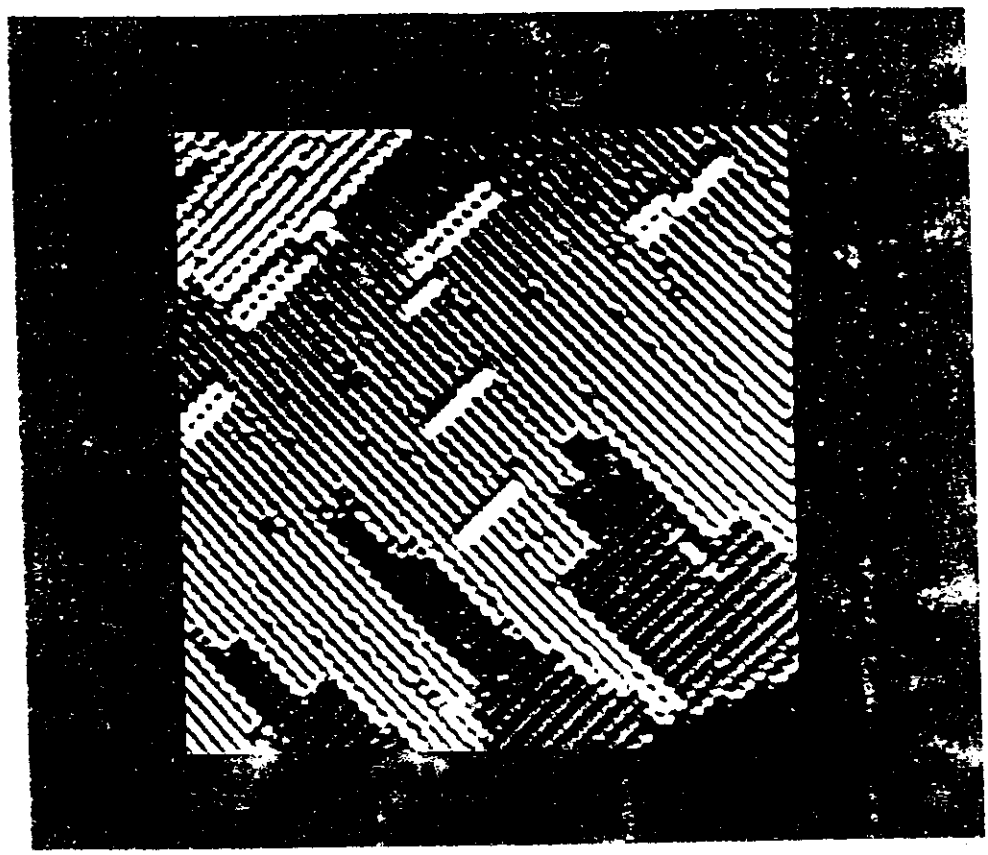

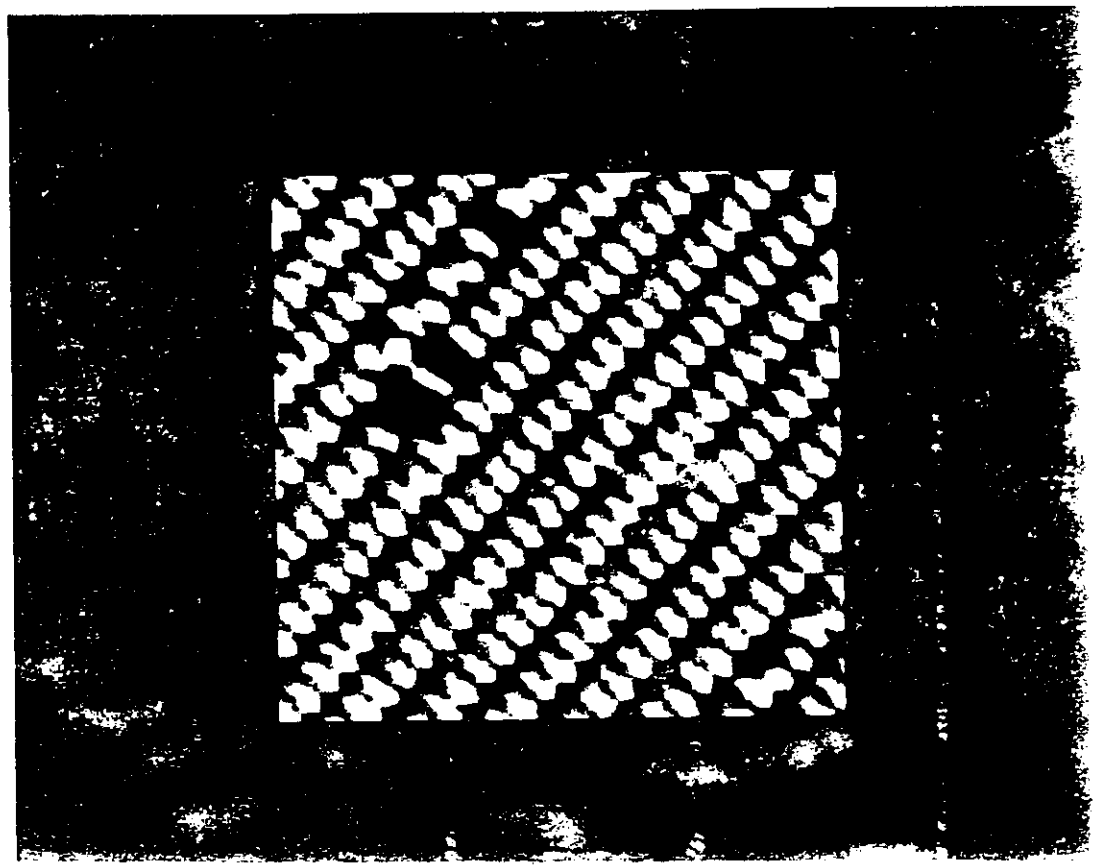

Nucleation, Growth, and Microstructural Evolution

Control variables:

* film material
* flux and chemical state of incident particles
* kinetic energy of incident particles
* particle angle of incidence
* flux, chemical state, and kinetic state of incident contamination
* substrate crystallinity, orientation, reconstruction, and surface perfection
* substrate surface cleanliness
* film growth temperature

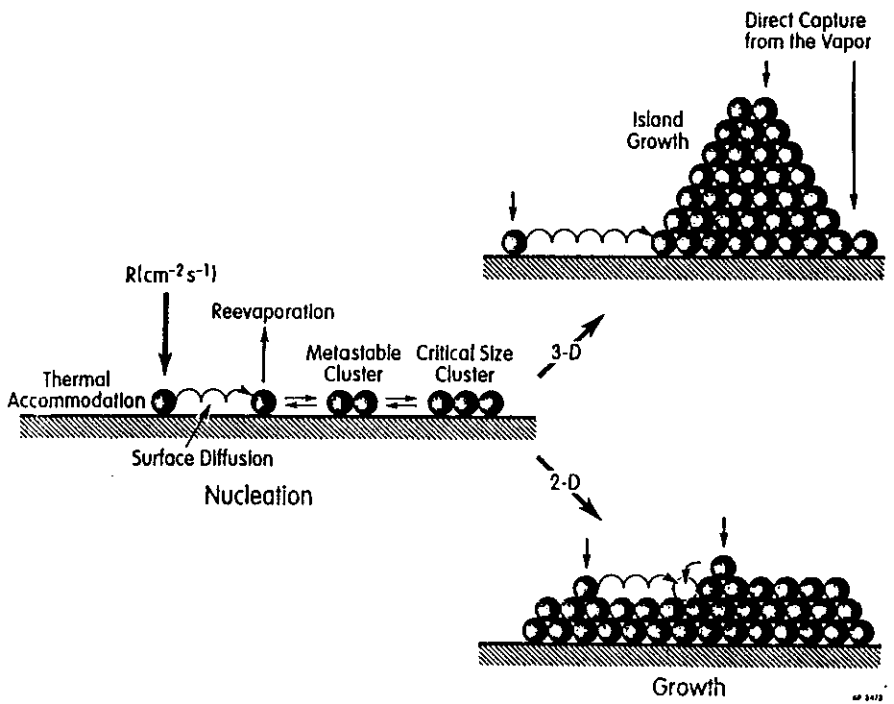

Homogeneous Capillarity Model of Nucleation

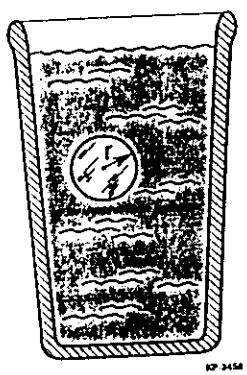

Example: nucleation of solid ice in pure water at $T \leq T_{mp}$. Assume ice nuclei is spherical with radius r.

$$\Delta G_{tot} = 4\pi r^2\gamma + 4/3(\pi r^3)\Delta G_V \quad \ldots\ldots\ldots\ldots\ldots\ldots \quad (1)$$

Where: ΔG_V = volume free energy of the nuclei (negative)
γ = net change in surface free energy (positive).

Set $\partial\Delta G/\partial r = 0$ and solve for the critical cluster size,

$$r^* = -(2\gamma/\Delta G_V) \quad \ldots\ldots\ldots\ldots\ldots\ldots\ldots\ldots \quad (2)$$

Substitute (2) into (1) to obtain the free energy activation barrier,

$$\Delta G^*_{tot} = 16\pi\gamma^3/3(\Delta G_V)^2 \quad \ldots\ldots\ldots\ldots\ldots\ldots \quad (3)$$

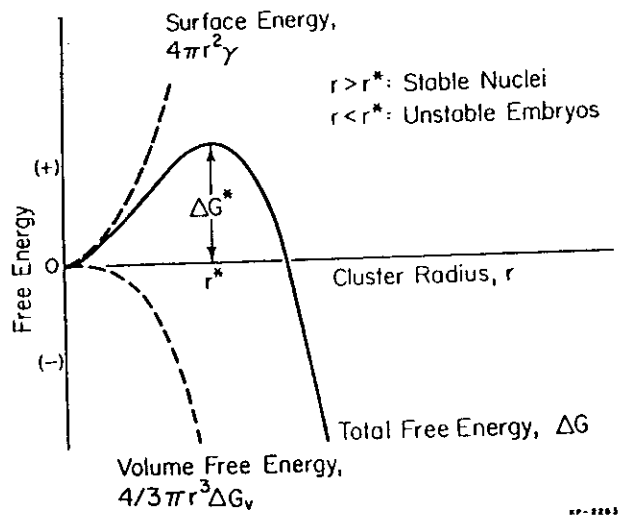

$$\Delta G^*_{tot} = 16\pi\gamma^3/3(\Delta G_V)^2 \quad \text{and} \quad r^* = -(2\gamma/\Delta G_V)$$

By definition, $\Delta G_V = \Delta H_V - T\Delta S_V$.

Near T_c, Trouton's rule gives $\Delta H_V \simeq T_c\Delta S_V$. Thus,

$$\Delta G_V \simeq \Delta H_V[(T_c - T)/T)] \quad \ldots\ldots\ldots\ldots\ldots\ldots \quad (4)$$

$\therefore$ r* decreases as: (1) T decreases below T_c and (2) ΔH_V increases (e.g. refractory metals such as W, Mo, and Ta).

Within the same simple framework, now consider the nucleation of a new solid phase on a substrate due to the impingement of a flux of atoms from the vapor phase.

A general expression of the combined first and second laws of thermodynamics is

$$d(\Delta G) = VdP - SdT \quad \ldots\ldots\ldots\ldots\ldots\ldots\ldots\ldots \quad (4)$$

where V and S are the system volume and entropy, respectively. Substituting the ideal gas law PV = NkT at constant temperature yields

$$d(\Delta G)\big|_T = NkT(dP/P).$$

Consider the addition of a single adatom on the substrate which is maintained at T_s. Then, since ΔG_V is just $\Delta G/\Omega$ where Ω is the adatom volume,

$$d(\Delta G_V)\big|_T = [kT_s/\Omega](dP/P), \text{ or}$$

$$\Delta G_v = [kT_s/\Omega]\ell n(P/P_{vp}) = [kT_s/\Omega]\ell n(\zeta) \quad \ldots\ldots\ldots\ldots \quad (5)$$

where P_{vp} is the equilibrium vapor pressure of the solid phase at temperature T and ζ is the supersaturation at the growth surface (i.e., the ratio of the arriving and desorbing fluxes).

Substituting (5) into (2) yields

$$r^* = 2\Omega\gamma/kT_s\ell n(\zeta) \quad \ldots\ldots\ldots\ldots\ldots\ldots\ldots\ldots \quad (6)$$

Thus, r^* decreases as ζ increases (i.e., as T_s decreases since $P_{vp} \propto \exp[(-\Delta H_{sub})/kT_s]$).

Examples of Critical Nuclei Size

1. Classical TEM experiments with Au/NaCl ⇒ r^* = 2-3 atoms at 300 K.

   $r^* = 2\Omega\gamma/kT_s\ell n(\zeta)$

   Au: fcc, a_o = 4.078 Å, r = 1.44 Å, γ_{Au} = 1400 ergs cm^{-2} (≃ 1.75 eV/atom), ζ(300 K) ≃ 2×10^4.
   NaCl: γ_{NaCl} = 227 ergs cm^{-2} (≃ 0.28 eV/atom).

   $r^* = 2[(4/3)\pi(1.44\text{Å})^3][(1400\text{-}227)\text{ergs-cm}^{-2}](1.6\times10^{-12}\text{ergs-eV}^{-1})^{-1}(10^{-16}\text{ cm}^2\text{ Å}^{-2})\,/(8.617\times10^{-5}\text{ eV K}^{-1})(300\text{ K})\ell n(2\times10^4)$

   $r^* = 7.15$ Å.

   (γ values from G. Samorjai, *Chemistry in Two Dimensions*, Cornell Press, Ithaca, NY, 1981).

2. TEM replica investigations of Zn deposition on glass.

   Zn: hcp, r = 1.38 Å, T_{mp} = 419.5 °C (693 K), P_{vp}(300 K) ≃ 10^{-12} Torr (≃ 10^8 cm^{-2} s^{-1}), P_{vp}(685 K) ≃ 10^{-1} Torr (≃ 5×10^{19} cm^{-2} s^{-1}).

T_s (K)	T_s(°C)	r^* (Å)
300	27	3.3
685	412	240

Heterogeneous Capillarity Model of Nucleation

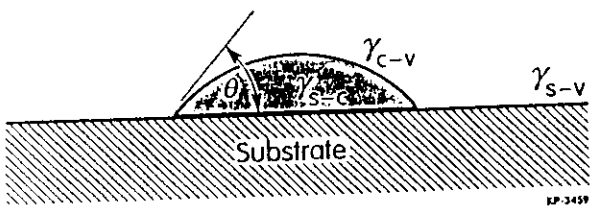

Assume that a spherical-cap cluster of mean dimension r and contact angle θ forms on a solid surface due to deposition from the vapor phase. The cluster has a surface area a_1r^2 exposed to the vapor phase, a contact area a_2r^2 with the substrate, and a volume a_3r^3 where the a_i terms are constants of geometry. The total free energy of the cluster with respect to dissociation into the vapor phase is

$$\Delta G = a_1r^2\gamma_{c\text{-}v} + a_2r^2\gamma_{s\text{-}c} - a_2r^2\gamma_{s\text{-}v} + a_3r^3\Delta G_v \quad \ldots\ldots\ldots\ldots (1)$$

where:

$\gamma_{c\text{-}v}$ = the positive free energy associated with the formation of a new surface between the condensate and the vapor phase.

$\gamma_{s\text{-}c}$ = the positive or negative surface free energy between the substrate and the condensate.

$\gamma_{s\text{-}v}$ = the positive free energy of the free substrate surface.

ΔG_v = the negative volume free energy of the nuclei.

(Note: perfect wetting, 2D growth, corresponds to $\theta = 0$; but θ may be thickness dependent).

$$\Delta G = a_1r^2\gamma_{c\text{-}v} + a_2r^2\gamma_{s\text{-}c} - a_2r^2\gamma_{s\text{-}v} + a_3r^3\Delta G_v$$

There are three equilibrium limits to equation (1).

1. **3D island (Volmer-Weber) growth:**

$$a_2r^2\gamma_{s\text{-}v} < [a_2r^2\gamma_{s\text{-}c} + a_1r^2\gamma_{c\text{-}v}].$$

In other words, the net surface free energy associated with the formation of a cluster is positive. This leads directly to the establishment of a free energy barrier.

2. **2D (Frank-van der Merwe) layer growth:**

$$a_2r^2\gamma_{s\text{-}v} \geq [a_2r^2\gamma_{s\text{-}c} + a_1r^2\gamma_{c\text{-}v}].$$

In this case, there is, in principle, no barrier to nucleation. In the presence of steps, growth can proceed with ζ approaching unity.

3. **Stranski-Krastanov growth** (intermediate case with 2D → 3D transition):

$$a_2r^2\gamma_{s\text{-}v} \approx [a_2r^2\gamma_{s\text{-}c} + a_1r^2\gamma_{c\text{-}v}].$$

The 2D → 3D transition can be driven by increasing stress in the overlayer as a function of film thickness due to, for example, coherency strain arising from film/substrate lattice mismatch.

Coverage / Mechanism	θ < 1ML	1 < θ < 2	θ > 2 > ML	Examples
3-D Island Growth				Metals on a-SiO_2
2-D Layer-by Layer Growth				Cd/W, AlAs/GaAs
Stranski-Krastanov Growth				In/Si, Ag/Si, Ge/Si

KP-2781

Mean-Field Minimal Rate Theories for 2-D Nucleation and Island Growth

Assume, for simplicity, 2D epitaxial growth on a terrace at a growth temperature and deposition rate for which the smallest stable island is a dimer. Furthermore, assume:

- desorption is negligible ($S_{3\text{-}D} \approx 1$).
- the capture probability σ for a diffusing adatom incident at a stable island is unity ($S_{2D} \approx 1$).
- the adatom concentration n is $\ll N$, the island concentration.
- the coverage θ is such that the coalescence rate is not significant.

Then,

$$\frac{dn}{dt} = J - \sigma D_s n N \qquad (1)$$

$$\frac{dN}{dt} = D_s n^2 \qquad (2)$$

At steady state, from (1)

$$J = \sigma D_s n N \qquad (3)$$

Substitute (3) into (2) for n:

$$\int i^2 dN = \int \frac{J^2}{\sigma^2 D_s}\, dt \qquad (4)$$

where:

$$\theta = \frac{Jt}{N_s}$$

$$\therefore dt = \frac{N_s}{J} d\theta \qquad (5)$$

Substitute (5) into (4) and solve:

$$\boxed{N(\theta) = \left(\frac{J}{D_s}\right)^{1/3} \left(\frac{3 N_s \theta}{\sigma^2}\right)^{1/3}}$$

Thus, for a given coverage, when $n \ll N$,

$$\boxed{N \propto \left(\frac{J}{D}\right)^{1/3}}$$

See: A. Zangwill, J. Cryst. Growth 163, 8 (1996).

For the more general case, a variety of scaling laws have been derived. The most important ones, in terms of fitting experimental data are:

$$N \propto \left(\frac{J}{D_s}\right)^p \quad \text{where} \quad \begin{cases} p = \frac{i+1}{i+3} & N \simeq n \\ p = \frac{i}{i+2} & N >> n \end{cases}$$

where $(i+1)$ is the smallest stable island size and i is in units of atoms.

Thus, to the extent that the models are correct, measuring the exponent p provides some insight into nucleation mechanisms. Note, however, that in addition to the rather restrictive assumptions mentioned initially, σ is generally a $f(\theta)$ and this must also be accounted for.

For references, see:

1. MJ Stowell, Phil. Mag 21, 125 (1970)
2. S. Stoyanov and D. Kashchiev, in "Current Topics in Materials Science," ed. by E. Kaldis, Vol. 7 (North Holland, Amsterdam, 1981), p. 69.
3. JA Venables, GDT Spiller, and M. Hanbucken, Rep. Prog. Phys. 47, 399 (1984).
4. L.-H. Tang, J. Phys. I 3, 935 (1993).

Cu/Cu(001)
$T_s = 223$ K

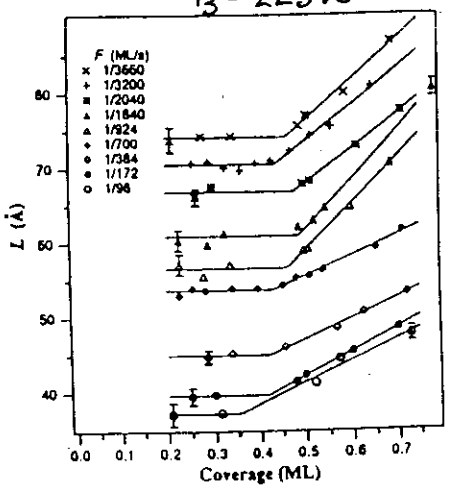

FIG. 2. Island separation vs coverage for various fluxes at a fixed $T = 223$ K, where solid lines are fits of two connected line segments to the data.

$L \propto \frac{1}{N^{1/2}}$ where L = average island separation

but $N \propto \left(\frac{J}{D_s}\right)^p$

$\therefore \boxed{L \propto \left(\frac{D_s}{J}\right)^{p/2}}$

J-K Zuo, J.F. Wendelken, H. Dürr, and C-L Liu, Phys. Rev. Lett. 72, 3064 (1994).

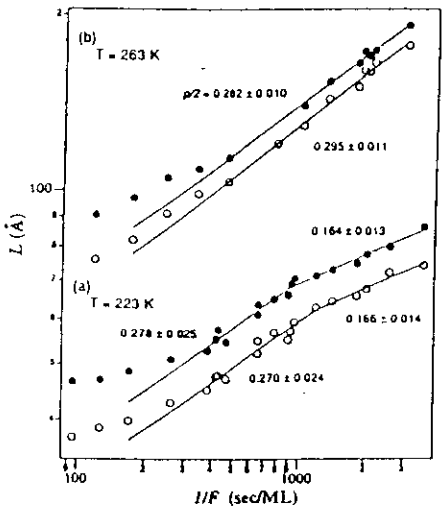

FIG. 3. The log-log plots of island separation vs inverse flux, where the slope gives $p/2$ with the value marked in each data regime: (a) $T = 223$ K and (b) $T = 263$ K. Open circles correspond to $\theta = 0.3$ ML. Solid circles correspond to $\theta = 0.63$ and 0.70 ML, for temperatures of 263 K and 223 K, respectively.

$T_s = 263$ K

In the steady state regime where L is constant (open circle data pts, $\theta \approx 0.3$ ML), i.e. $N >> n$

$$p \approx \frac{3}{5} = \frac{i}{i+2} \Rightarrow i = 3$$

$\therefore$ smallest stable island = **tetramer**

$T_s = 223$ K

In steady-state with $1/J \gtrsim 1000$ s/ML (or $J \lesssim 10^{-3}$ ML/s (!)!

$$p \approx \frac{1}{3} = \frac{i}{i+2} \Rightarrow i = 1$$

$\therefore$ smallest stable island = **dimer**

Note that at higher J, there is a shift to $p \lesssim 1/2$ which is not understood.

Solid-on-Solid Film Growth Model

SOS is a simple discrete atomistic growth model which allows ballistic deposition on the tops of randomly-chosen atomic columns in a crystallographic array, followed by relaxation through surface diffusion to higher coordinated sites. Thus, overhangs, atomic shadowing, and vacancies are not allowed. The effects of deposition rate is accounted for by changing the number of surface sites visited.

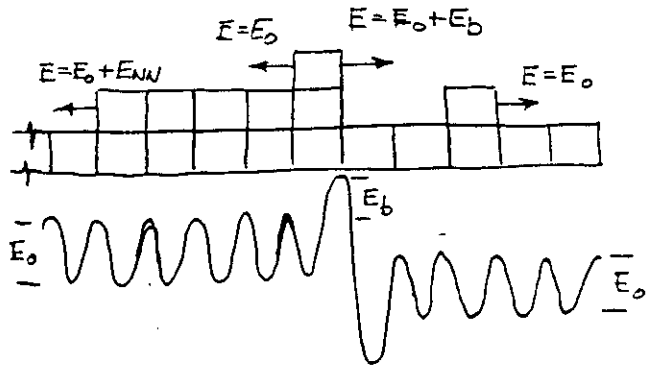

1-D view of SOS relaxation processes

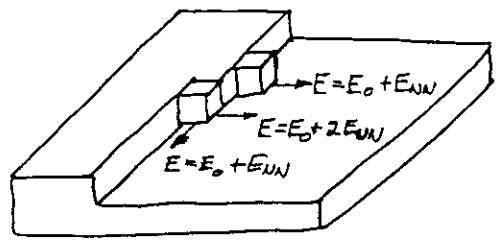

2-D view

$\theta = \underline{0.2}$ ML

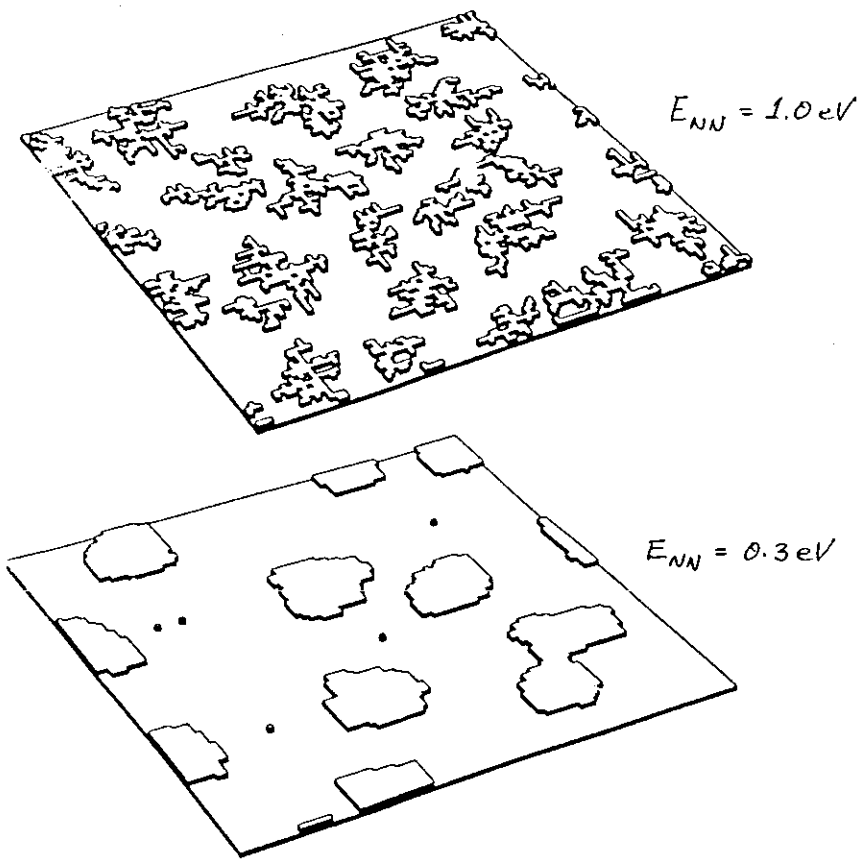

C. Ratsch et al. PRL 72, 3194 (1994)

Pt/Pt(111)
$R = 10^{-2}$ ML/s

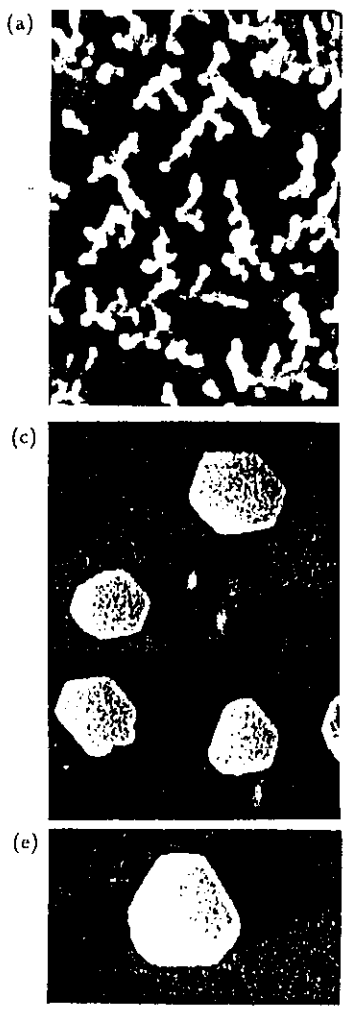

T_S = 200 K
θ = 0.2 ML

T_S = 455 K
θ = 0.14 ML

T_S = 710 K
θ = 0.08 ML

T. Michely et al., PRL 70, 3943 (1993)

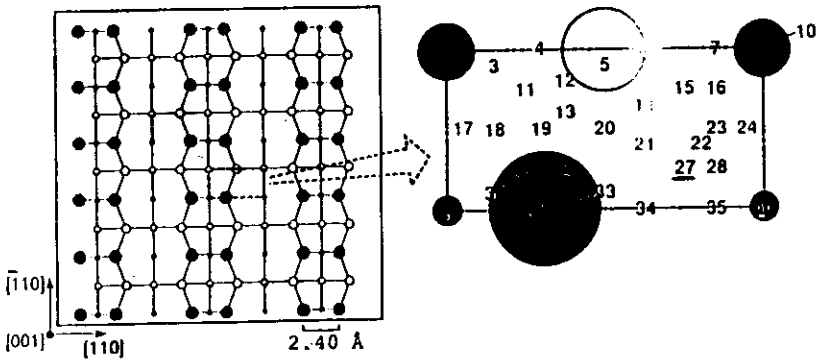

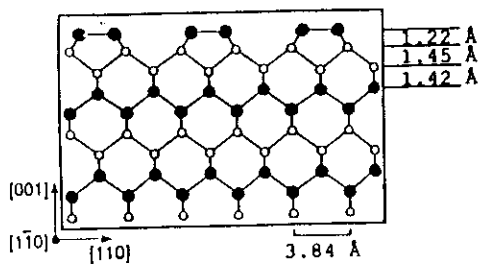

- 1st layer atom
- 2nd layer atom
- 3rd layer atom
- 4th layer atom

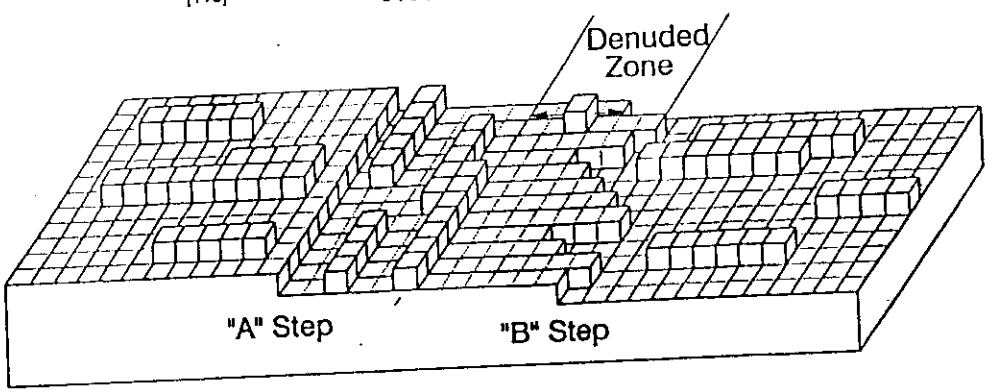

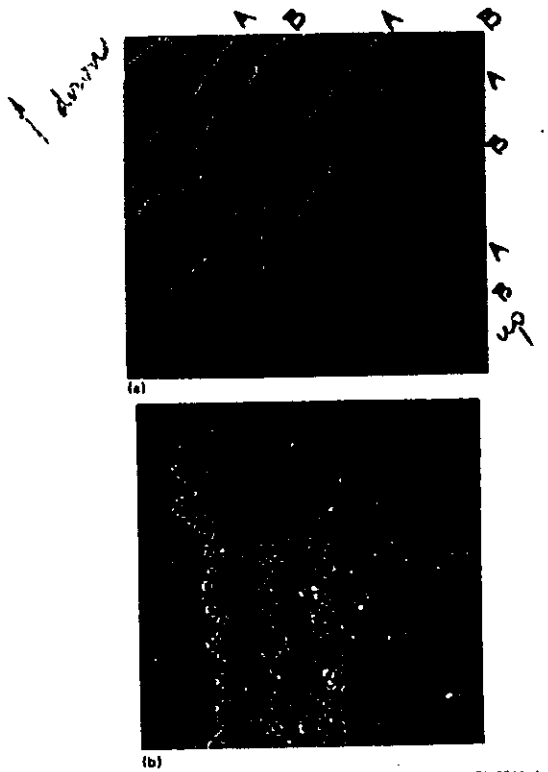

FIG. 1. STM micrograph of the clean surface of nominally flat Si(001). (a) Low magnification, scale: 3500 × 3500 Å, taken in derivative mode. (b) Higher magnification, scale 350 × 350 Å. In both views the highest terrace is at lower right. In view (a) dimer rows run parallel and perpendicular to the picture diagonal on alternate terraces. The smooth edges occur when the dimer rows are parallel to the edge.

Anisotropic diffusion, $E_s \approx 40$ meV

Anisotropic accomodation

"A" step = upstairs dimer rows parallel to the edge; high energy
"B" step = " " " ⊥ " " " ; low energy

Mo, Kariotis, Swartzentruber, Webb, and Legally
J. Vac. Sci. Technol. A8, 201 (1990).

and

Phys. Rev. Letters 63, 2393 (1989).

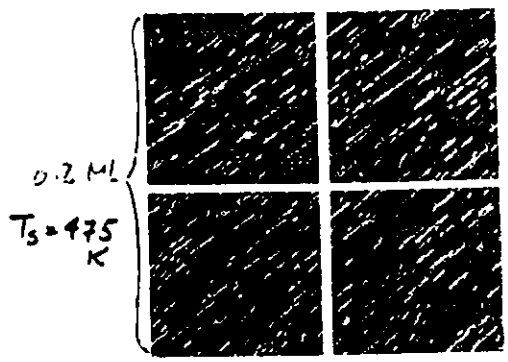

FIG. 3. STM micrographs of the uniformity of deposition. Each panel is from a different substrate area for a particular deposition: 475 K, 0.2 ML dose, rate 1/200 ML/s. To obtain good statistics for determining the diffusion coefficient, island densities in 10 or more such areas are averaged.

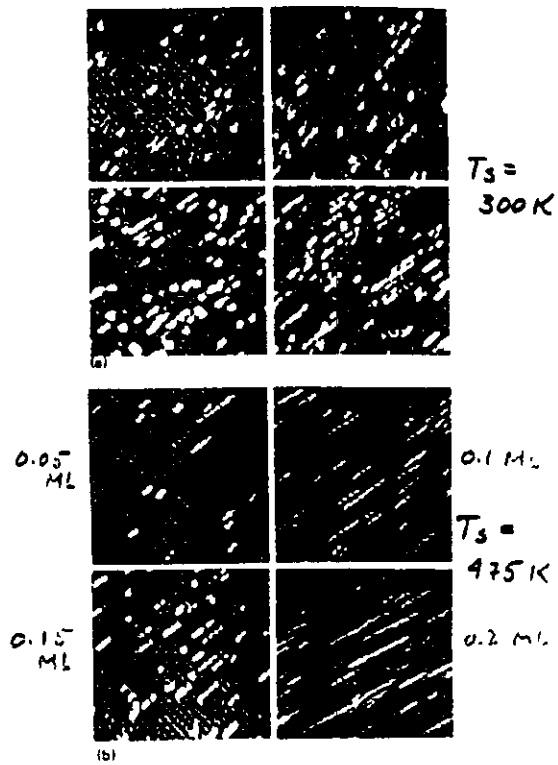

FIG. 2. STM micrographs of island distribution in two sequences of growth at a rate of 1/200 ML/s. (a) 300 K, (b) 475 K. The four panels in each view represent doses of 0.05 monolayers (ML), 0.1, 0.15, and 0.2 ML. The island density increases as the dose increases. Island shapes are anisotropic, and more anisotropic at the higher temperature. Scale: 230 × 230 Å, each panel.

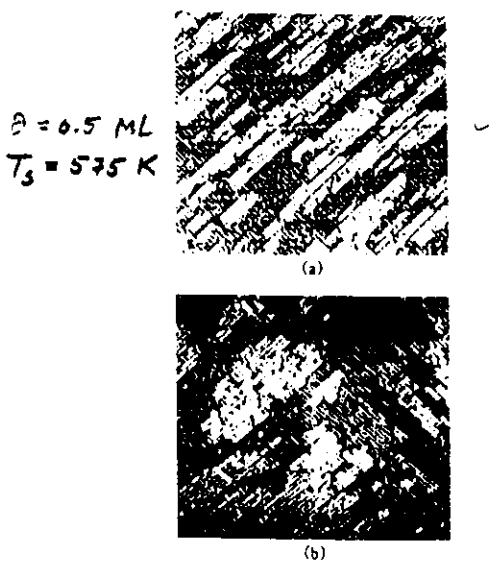

FIG. 3. STM micrographs of island structure for deposition of 0.5 ML of Si at 1/20 ML/sec and 575 K; (a) as deposited and (b) after annealing for 10 min at 575 K. Scale is 500 × 500 Å^2. Islands become more rounded with annealing.

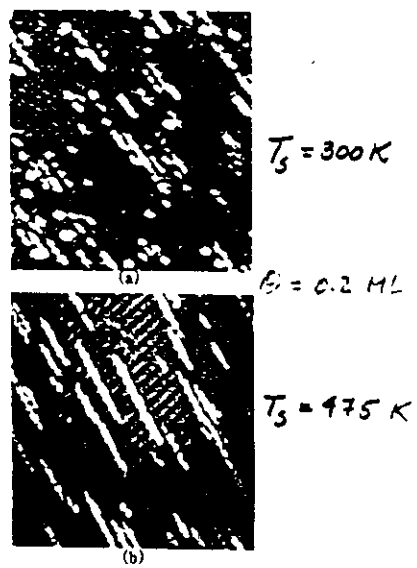

FIG. 1. STM micrographs of island shapes and distributions for growth at a rate of 1/200 ML (monolayer) per second to a coverage of 0.2 ML at (a) 300 K and (b) 475 K. Islands are long in the direction of a dimer row. The anisotropy depends on deposition rate and substrate temperature. Scale, 230 × 230 Å^2.

Terraces

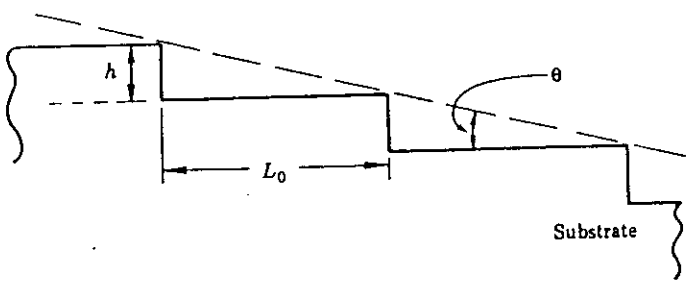

$$\ell = h/\tan(\theta)$$

For Si, with a lattice constant a_o = 5.43 Å, single-atom-height (i.e. monolayer) steps on the (001) surface correspond to h = $a_o/4$ = 1.36 Å. Even the best aligned substrates have miscuts of ≥ 0.1° corresponding to average terrace widths of = 780 Å.

θ (deg)	ℓ (Å)
0.1	779
0.5	156
1	80
2	39

Si(001)2×1
Miscut ≃ 0.4°
Scan = 2000Å × 3800Å
V_S = −2V

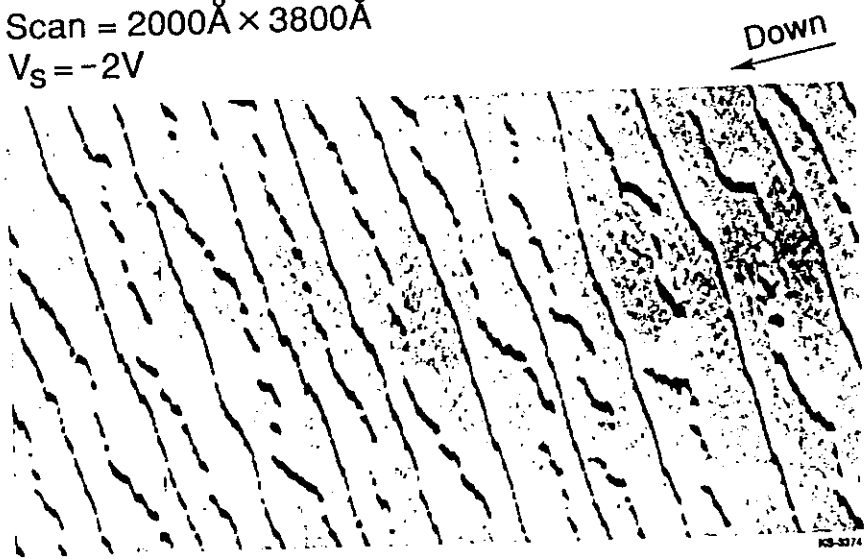

Lin, Hirschorn, Chiang, Tsu, Lubben, and Greene
Phys Rev. B46, 3494 (1992).

Assume that surfaces do not reconstruct i.e. dangling bonds don't rehybridize into pairs or higher-order atomic arrangements. At low to medium T_s, the dominant features are the terraces (planar 2-D defects in a bulk 3-D crystal) separated by steps, or ledges, which are 1-D line defects on a 2-D surface. The steps themselves are not straight and have defects called kinks which are point defects in 1-D steps.

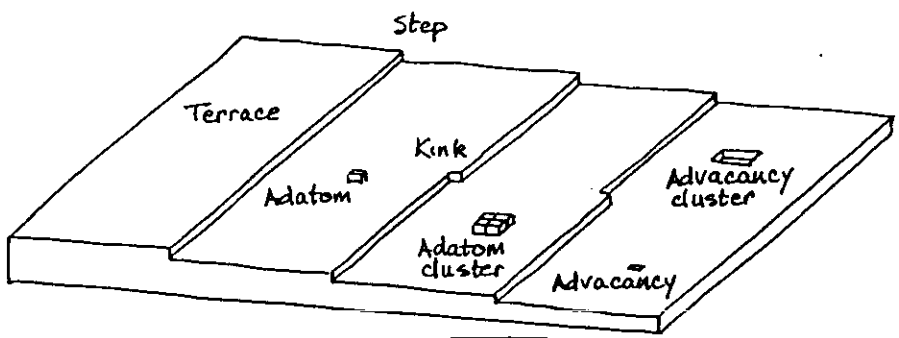

Intrinsic 'Defects'	Dimensionality
Terraces	2-D
Steps	1-D
Kinks	0-D

'Extrinsic' Defects
Adatoms
Clusters
Vacancies
Vac-clusters

Consider putting $\theta = 0.5$ ML of adatoms on a large terrace. There are 2 extremes.

1. Clustering. In order to minimize the total enthalpy, the adatoms can cluster together into 2 half terraces and maximize the number of lateral in-plane bonds.

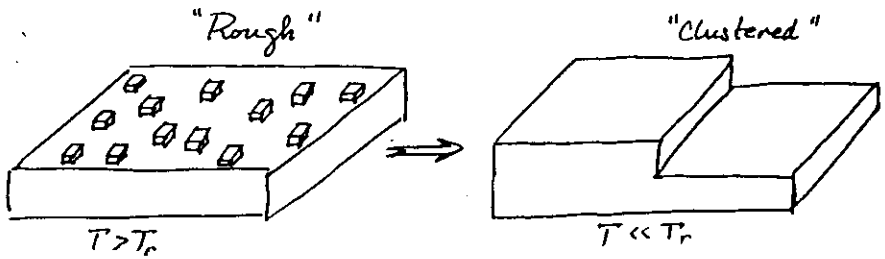

Single terrace with coverage θ.

2. Random distribution. The other extreme is that adatoms can maximize their configurational entropy and distribute themselves randomly.

The Helmholtz free energy per surface site is

$$f = u - Ts.$$

Thus, at low T the system (when allowed to proceed toward equilibrium) will tend toward the smooth (ie. clustered) case and at high T it will tend to roughen. At intermediate temperatures, a phase transition occurs at the microscopic roughening temperature T_R. This is akin to a miscibility gap in a binary 2-D "alloy" composed of adatoms and vacancies.

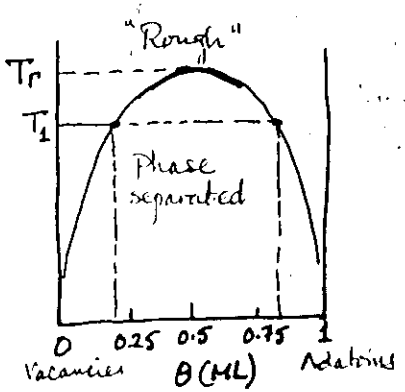

Low T → smooth
High T → rough

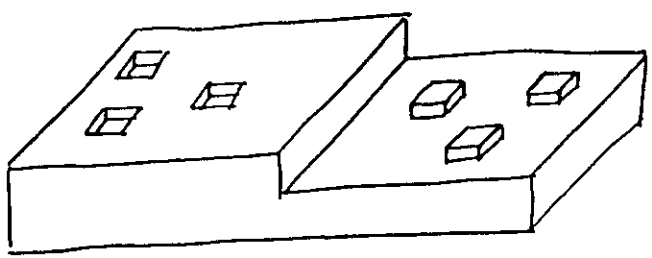

θ = 0.5 ML
$T = T_1$
(intermediate T)
⇒ 2 "mixed" phases by the "lever rule."

Surface	T_R (°C)	T_m (°C)	T_R(K)/T_m(K)
In(110)	20	118	0.69
Pb(110)	143	328	0.69
Ag(110)	638	962	0.74
Cu(110)	762B	1083	0.66
Ni(110)	7102B	1448	0.76

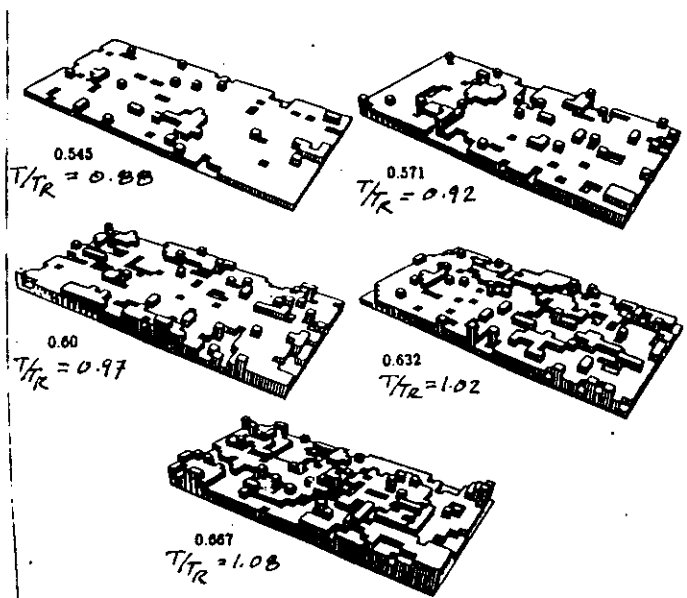

Isolated steps also have a roughening temperature, T_r^{step}, which is considerably lower than T_r. Isolated steps can have both positive and negative kinks and "wander" over the terrace. Kink-induced step-wandering is favorable in that it increases the entropy of the step but the kinks themselves cost energy. For example, in the figure below, moving an adatom from step position *a* to step position *b* results in the production of 4 kinks.

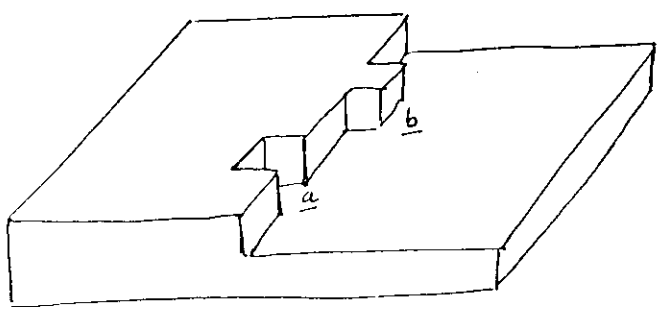

The number density of kinks is again determined by a balance between energetics and entropy

$$f_{step} = u_{step} - Ts_{step}$$

where f_{step} is the free energy per lattice unit of straight step length and

$$u_{step} = u_{kink}\, p + \epsilon_{step}.$$

ϵ_{step} is the energy per unit straight step length and p is the probability of producing a kink.

At $T = T_r^{step}$ the step energy vanishes and steps form spontaneously for $T \geq T_r^{step}$. STM images show that all surfaces contain steps which wander. In fact, for Si(001), the steps are alternately relatively smooth (type "A") and relatively rough (type "B"). Both types of steps (even the "smooth" ones) contain high densities of randomly distributed kinks.

Epitaxy

Epitaxy ≡ επι (epi = placed or resting upon) + ταξις (taxis = arrangement).

Epitaxy refers to the growth of single-crystal overlayers in such a way that the crystallographic orientations of the overlayer and substrate are related in some simple manner. The word was introduced into the scientific literature in 1928 (L. Royer, *Bull. Soc. Fr. Mineral Crystallogr.* 51, 7 (1928)), although the growth of epitaxial metal films on alkali-halide substrates was reported more than 50 years earlier.

Homoepitaxy refers to the case in which film and substrate are identical (e.g. Si on Si) while **heteroepitaxy** refers to the growth of an overlayer composed of a different material than the substrate (e.g. W on MgO(001)1x1: W(001)‖MgO(001) and W[1$\bar{1}$0]‖MgO[100]), Kimura, Petrov, Adibi, and Greene, *J. Cryst. Growth* 123, 344(1992).

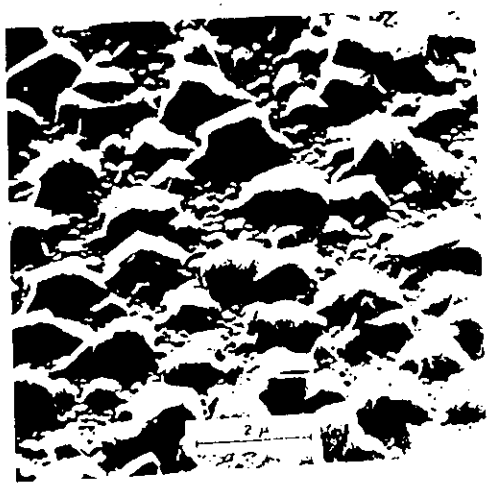

2D Growth

1. Step-flow growth

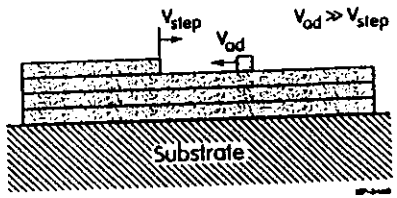

2. Layer-by-layer growth

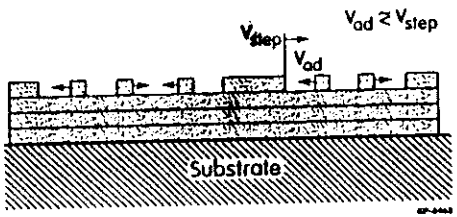

3. 2D multilayer growth

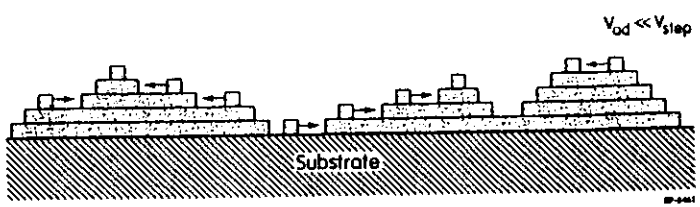

2D (Frank-van der Merwe) Layer Growth

1. Step-flow growth:

If adatom surface diffusion rates to step edges are much higher than adatom arrival rates and capture probabilities at single-atom-height steps are unity, then adatom coverages on terraces will be low, adatom-adatom interactions can be neglected, and growth proceeds by the flow of steps across the surface. Thus, the requirement for step flow growth is that

$$v_{ad} >> v_{step} \quad \ldots\ldots\ldots\ldots\ldots\ldots\ldots\ldots\ldots\ldots \quad (1)$$

where: $v_{ad} = D_s(\text{Å}^2\ s^{-1})/\ell(\text{Å})$
$v_{step} = R(\text{ML}\ s^{-1})\ell(\text{Å})$.

Thus,

$$D_s >> R\ell^2 \quad \ldots\ldots\ldots\ldots\ldots\ldots\ldots\ldots\ldots\ldots \quad (2)$$

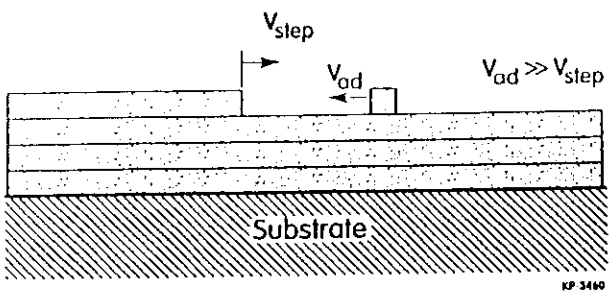

Another approach leading to the same conclusion is to note that step flow requires that $(D_s\tau)^{1/2} >> \ell$ where $\tau = \{R(\text{atoms/s})\}^{-1}$.

Si(001)2×1
Miscut ≃ 0.4°
Scan = 2000Å × 3800Å
V_S = −2V

Lin, Hirschorn, Chiang, Tsu, Lubben, Greene
Phys Rev B 45, 3494 (1992).

Down

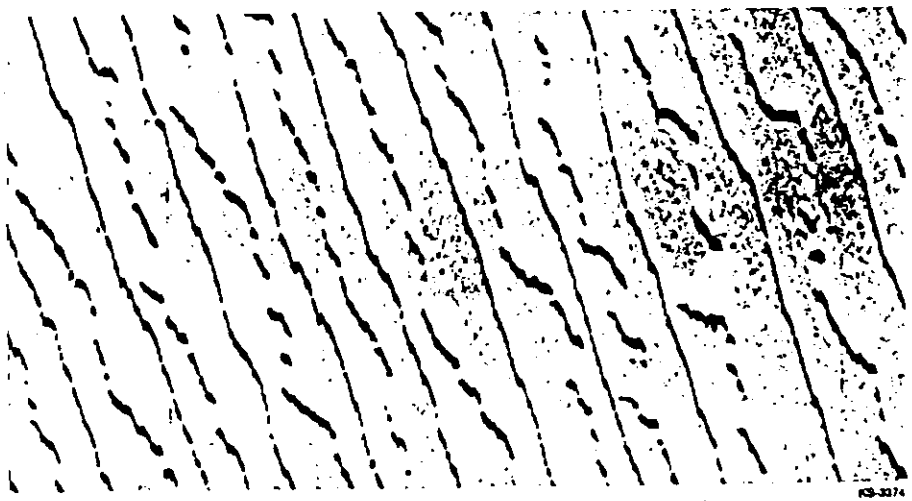

Step Periodicity vs Buffer Layers

Terrace size distributions on even the best polished or cleaned substrates are never uniform. However, they can be made more uniform, and hence the surface can be made microscopically smoother (important for the deposition of thin heteroepitaxial layers) by depositing a buffer layer under step-flow growth conditions. That is, under deposition conditions leading to adatom velocities being higher than step velocities and for which there are few adatom/adatom collisions on open terraces. The required conditions are: high T_s, low R, and excellent vacuum.

That this in fact occurs was first shown for GaAs MBE by Al Cho and John Arthur (see Prog. Sol. St. Chem. 10, 175 (1975)) by RHEED and TEM.

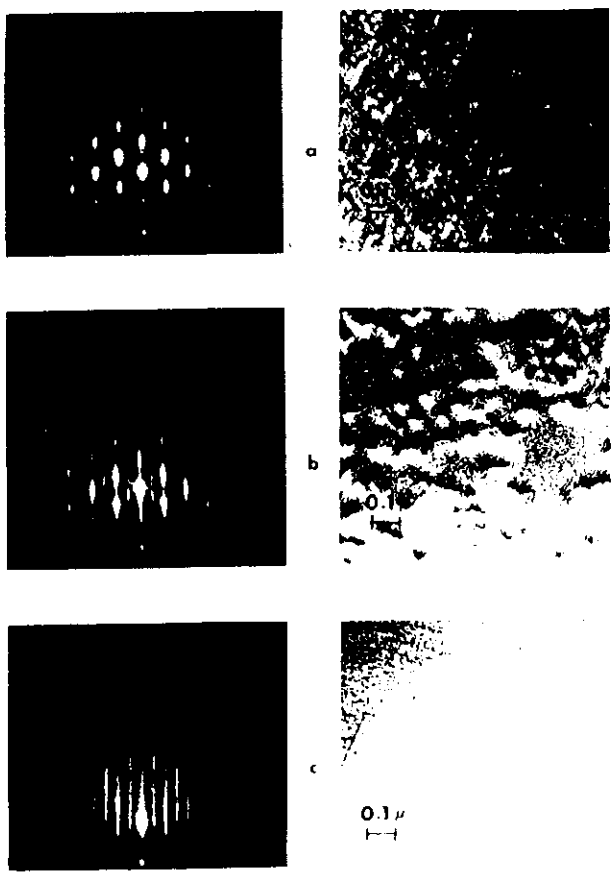

Consider the case of Si MBE on Si(001)2x1 for which adatom diffusion coefficients have been estimated through analyses of STM images as a $f(\theta,T_s)$. The result (Y.W. Mo et al., Surf. Sci. 268, 275 (1992)) is:

$$D_s\ (cm^2\ s^{-1}) \approx 10^{-3\pm1} \exp\left(\frac{-0.67\pm0.08\,eV}{kT_s}\right).$$

At T_s = 600 °C, $D_s \approx 1.4\times10^9$ Å^2 s^{-1}. Assume that the substrate is well aligned with a miscut of only 0.1°, corresponding to an average terrace length $\ell \approx 800$ Å.

Let: τ = time required to collect an adatom at a step edge from a distance $d = \ell/2$
R = 1 μm h^{-1} ≈ 2 ML s^{-1}
$\Delta\theta$ = accumulated Si coverage in time τ.

Then: $\tau = \langle d^2\rangle/D_s = (400\ Å)^2/(1.4\times10^9\ Å^2\ s^{-1}) = 1.2\times10^{-4}$ s
$\therefore\ \Delta\theta = R\tau = 2.4\times10^{-4}$ ML.

Thus, in principle, step flow is possible. For MBE Cu on Cu(001), de Miguel et al. (Surf. Sci. 189/190, 1062 (1987)) showed using He scattering that step flow occurs for $T_s \geq 420$ K (≈ 150 °C) where $D_s \approx 7\times10^7$ Å^2 s^{-1}.

Terrace Size Distributions During Step-Flow Epitaxy*

Observations:

1. Homoepitaxial high-temperature buffer layers reduce terrace size distributions (i.e. large terraces tend to shrink and small terraces tend to grow towards the average terrace size) and decrease surface roughness.
2. The fraction of atoms accumulated on each terrace is proportional to the terrace size.
3. FIM observations for metal atoms deposited on metal islands often indicate that the capture probability is higher at up-steps than at down-steps (although the transmission probability is higher at down steps).

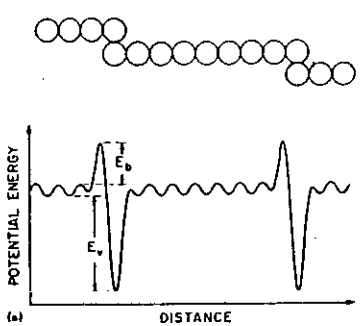

* 1. R.L. Schoebel, J. Appl. Phys. 40, 614 (1969).
2. R. Ghez and S.S. Iyer, IBM J. Res. Dev. 32, 804 (1988).
3. G.S. Bales and A. Zangwill, Phys. Rev. B41, 5500 (1990).
4. H.-J. Gossman, F.W. Sinden, and L.C. Feldman, J. Appl. Phys. 67, 745 (1990).
5. S.A. Chalmers, J.Y. Tsao, and A.C. Gossard, Appl. Phys. Lett. 61, 645 (1992).
6. P. Desjardins and J.E. Greene, J. Appl. Phys. 79, 1423 (1996).

Pt_7 Cluster on Pt(111)

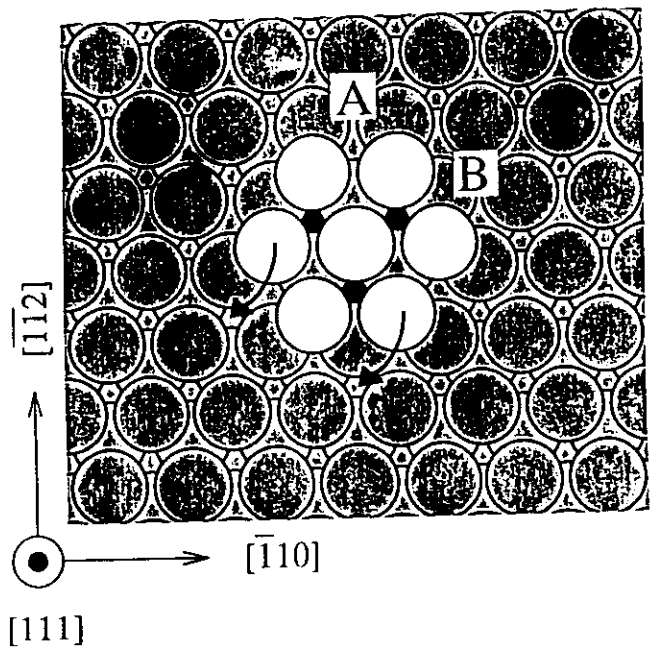

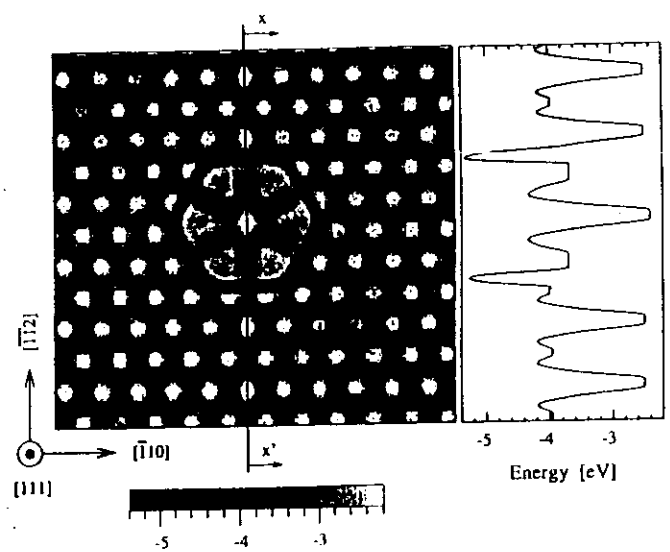

Terrace Size Distributions (Continued)

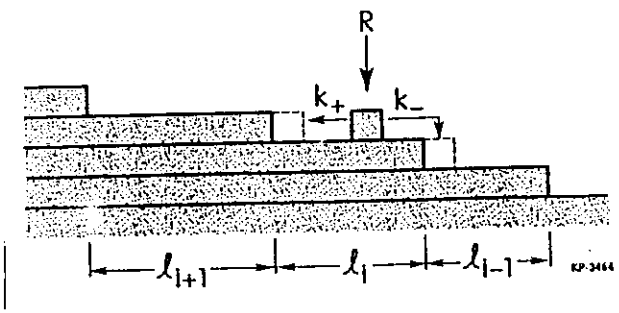

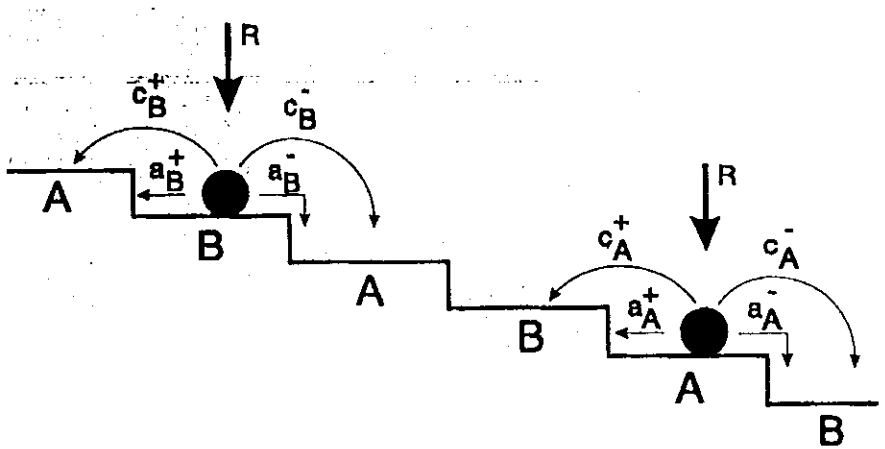

Model Calculations*:

1. Steps act as adatom sinks (large capture cross-sections with corresponding denuded zones). Diffusional anisotropy and dipole repulsive step-step interactions are ignored.
2. Terrace size distributions decrease during deposition only if $k_+ > k_-$. If $k_+ = k_-$, terrace size distributions increase without bound.
3. The width of the terrace size distribution asymptotically approaches zero (i.e. equal terrace sizes) very slowly. The best case corresponds to $k_+ = 1$ and $k_- = 0$, for which the width of the terrace size distribution approaches zero as $\theta^{-1/4}$.
4. Short wavelength perturbations (fluctuations) in terrace size distributions are damped faster than long wavelength perturbations.

$$a_x^+ + a_x^- + c_x^+ + c_x^- = 1 \qquad x = A, B$$

$$a_A = (a_A^+ + a_A^-) \; ; \; a_B = (a_B^+ + a_B^-)$$

$$\Delta a_A = (a_A^+ - a_A^-)/a_A \; ; \; \Delta a_B = \ldots$$

$$c_A = (c_A^+ + c_A^-) \; ; \; c_B = (c_B^+ + c_B^-)$$

$$\Delta c_A = (c_A^+ - c_A^-)/c_A \; ; \; \Delta c_B = \ldots$$

* P. Desjardins and J.E. Greene, J.Appl. Phys. 79, 1423 (1996).

Fig. 2

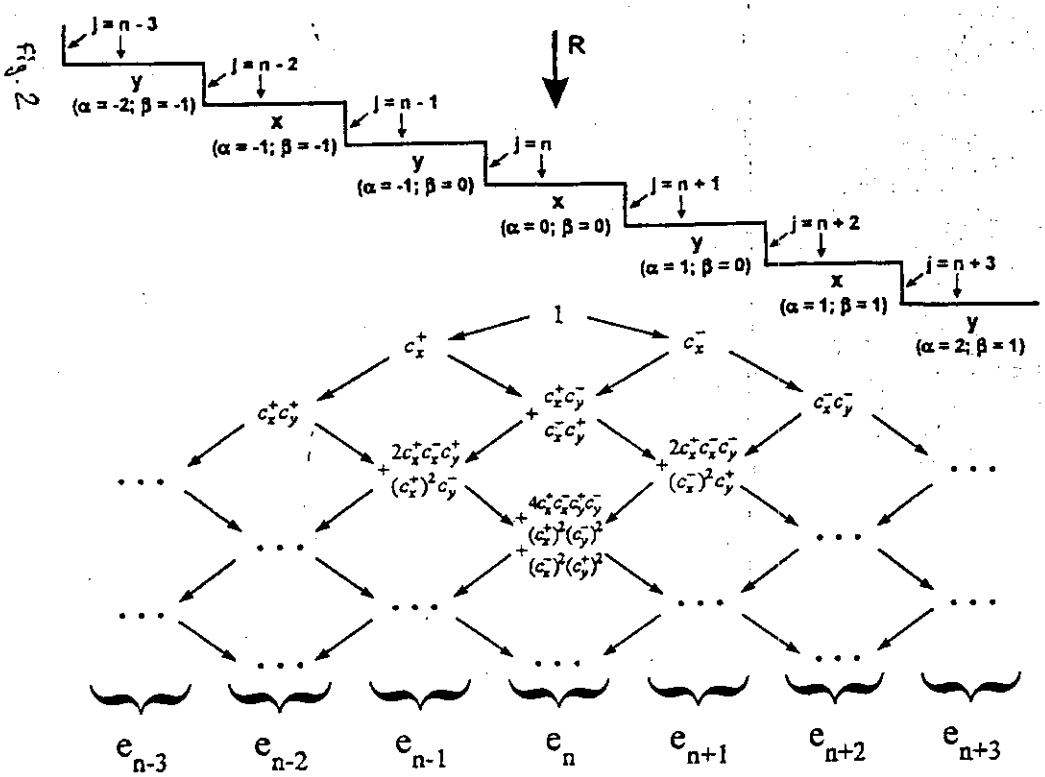

Consider the case in which the two types of terraces A and B are equivalent. Then, the number of encounters of an adatom incident on terrace n with terrace n+γ, where γ is the position of terrace j (i.e., the number of terraces away from terrace n), is

$$e_{n+\gamma} = \sum_{k=0}^{\infty} \binom{2k+|\gamma|}{k} \left(c_A^+ c_A^-\right)^k \left(c_A^\pm\right)^{|\gamma|} \qquad \gamma \le 0 \tag{1}$$

and

$$e_{n+\gamma} = \sum_{k=0}^{\infty} \binom{2k+|\gamma|}{k} \left(c_A^+ c_A^-\right)^k \left(c_A^\pm\right)^{|\gamma|}. \qquad \gamma \ge 0 \tag{2}$$

In these equations, k signifies the row number in a given column of the binomial distribution tree and corresponds to the minimum number of step crossings necessary to reach terraces in that row. The summation over k is then just the summation over all rows. The advancement ΔN of an ascending step on terrace j, where $j = n+\alpha+\beta$, of type x is then obtained from the number of adatom encounters, determined from equations (2) and (3), and the attachment coefficients for the adjacent terraces j and j-1,

$$\Delta N_{j,x} = e_{j-1}a_y^- + e_j a_x^+. \tag{3}$$

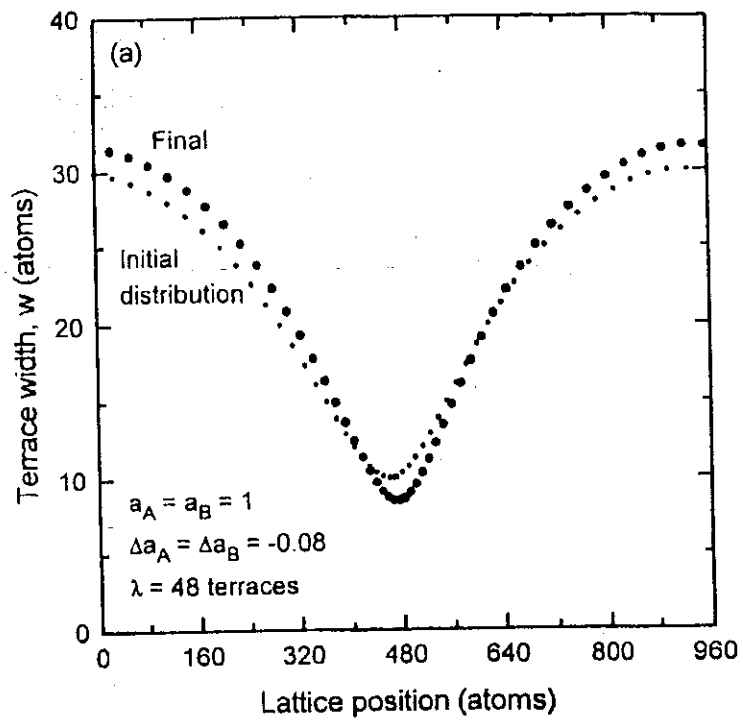
(a)
Final
Initial
distribution
$a_A = a_B = 1$
$\Delta a_A = \Delta a_B = -0.08$
λ = 48 terraces
Terrace width, w (atoms)
Lattice position (atoms)
0
10
20
30
40
0
160
320
480
640
800
960

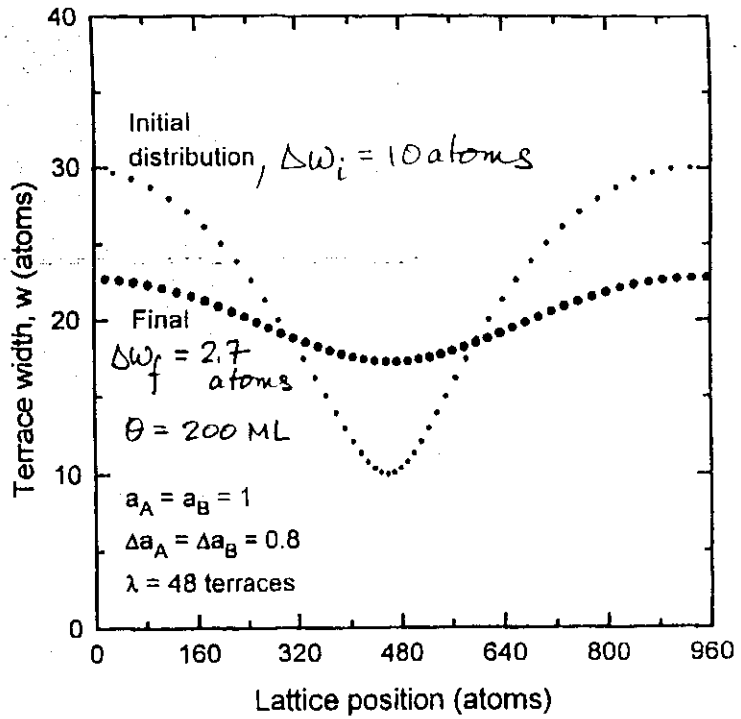
Initial
distribution, $\Delta\omega_i$ = 10 atoms
Final
$\Delta\omega_f$ = 2.7 atoms
θ = 200 ML
$a_A = a_B = 1$
$\Delta a_A = \Delta a_B = 0.8$
λ = 48 terraces
Terrace width, w (atoms)
Lattice position (atoms)
0
10
20
30
40
0
160
320
480
640
800
960

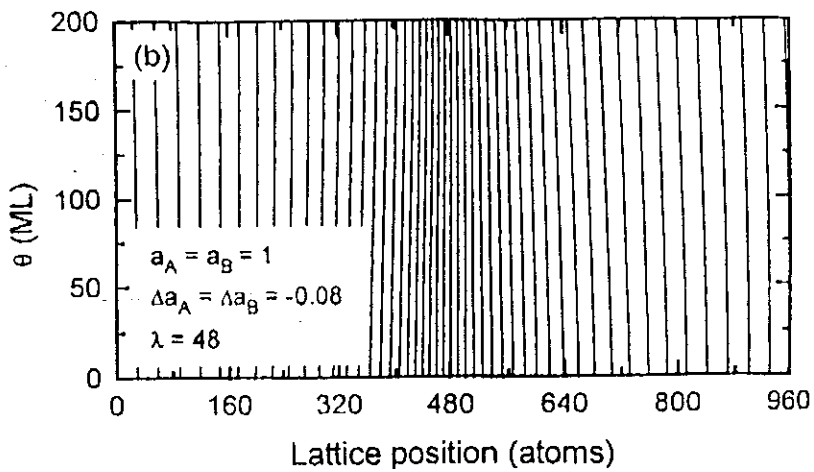
(b)
$a_A = a_B = 1$
$\Delta a_A = \Delta a_B = -0.08$
λ = 48
θ (ML)
Lattice position (atoms)
0
50
100
150
200
0
160
320
480
640
800
960

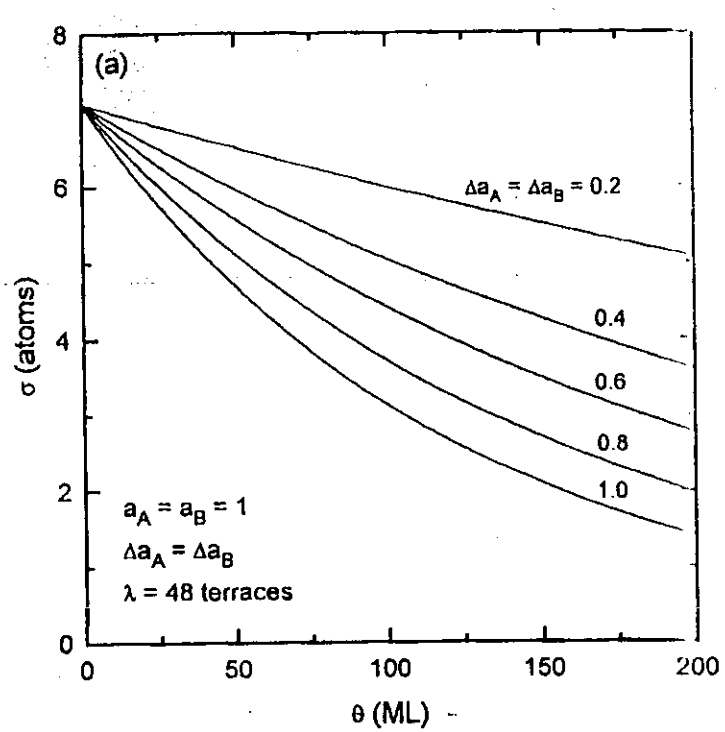
(a)
$\Delta a_A = \Delta a_B = 0.2$
0.4
0.6
0.8
1.0
$a_A = a_B = 1$
$\Delta a_A = \Delta a_B$
λ = 48 terraces
σ (atoms)
θ (ML)
0
2
4
6
8
0
50
100
150
200

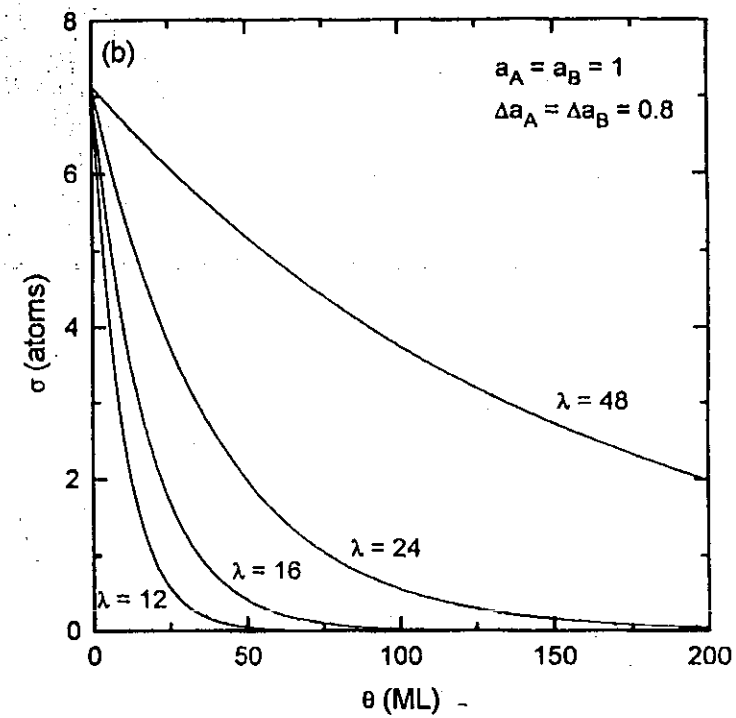
(b)
$a_A = a_B = 1$
$\Delta a_A = \Delta a_B = 0.8$
λ = 48
λ = 24
λ = 16
λ = 12
σ (atoms)
θ (ML)
0
2
4
6
8
0
50
100
150
200

2. **"Ideal" 2D layer-by-layer growth:**

For ideal layer-by-layer growth, new layers start to be formed only *after* the preceding layer is completed. Growth is thus truly two-dimensional and no more than two partial layers are exposed at any one time.

As adatom velocities decrease (through, for example, a decrease in T_s), the lattice-gas spreading pressure increases until at sufficiently high pressures, local density fluctuations lead to clustering and island formation (nucleation) on terraces *between* step edges. Clusters, which impede adatom mobilities, are continuously forming and dissolving. Some clusters become stable and continue to grow.

Cluster boundaries represent "extrinsic" steps which compete with "intrinsic" steps for adatoms.

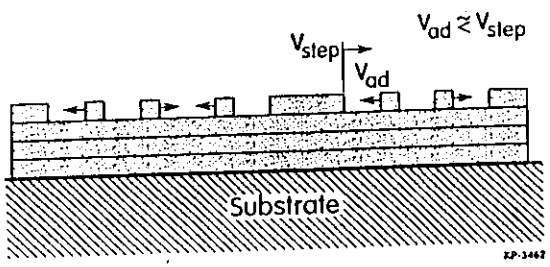

How can one distinguish between modes of 2-D epitaxial growth?

Low-angle diffraction intensity oscillations under conditions where **in-phase** diffuse scattering or out-of-phase elastic scattering intensities are sensitive to the presence of terrace step edges or islands.

* Electron diffraction (RHEED)
* X-ray diffraction
* Thermal particle scattering (TEAS)

In-phase oscillations -----> step edges
Out-of-phase oscillations -----> islands

Kinematic 2-Level Step Model

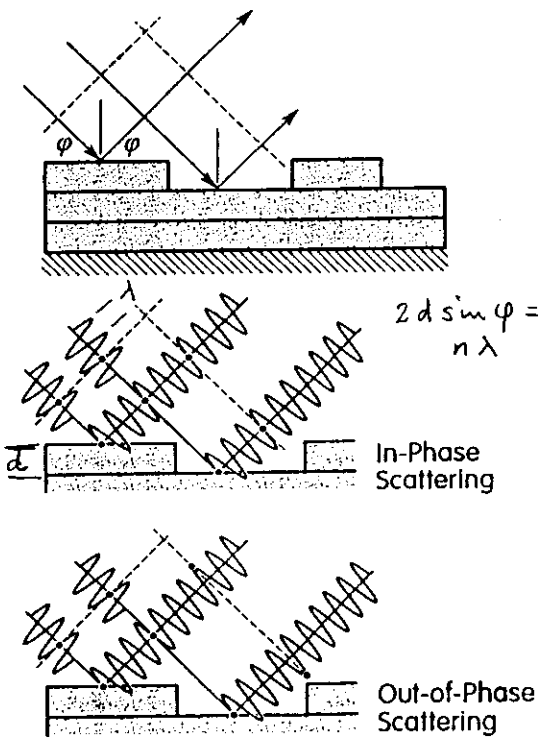

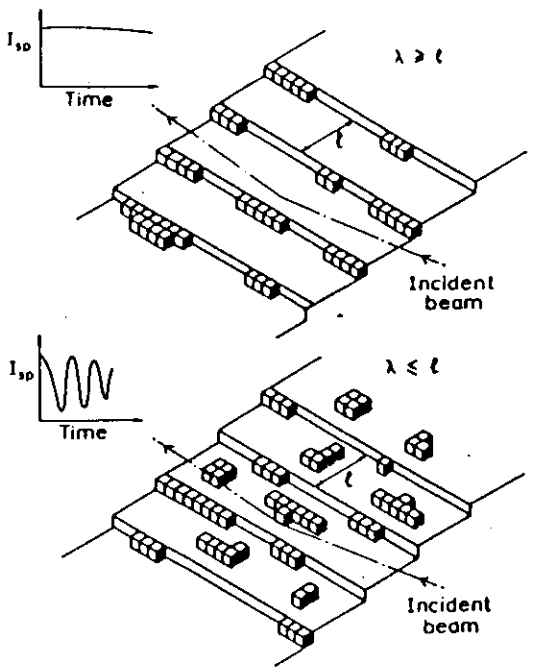

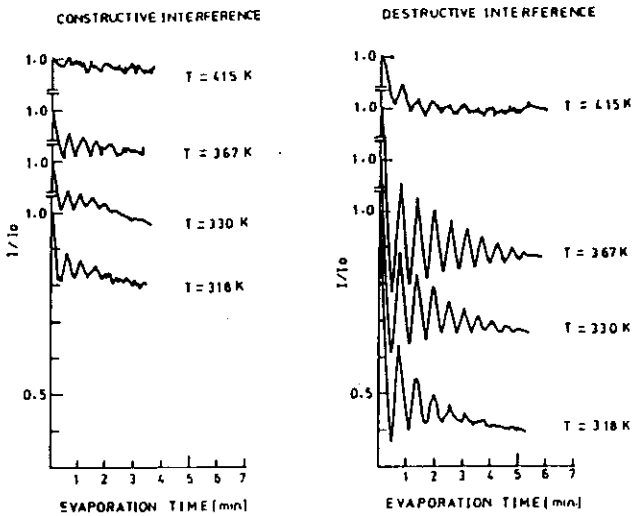

Fig. 1. Temporal evolution of the specularly reflected He intensity (normalized to the intensity before deposition) as a function of deposition time for different surface temperatures. The scattering conditions were chosen to be in-phase (left-hand side) and out-of-phase (right-hand side).

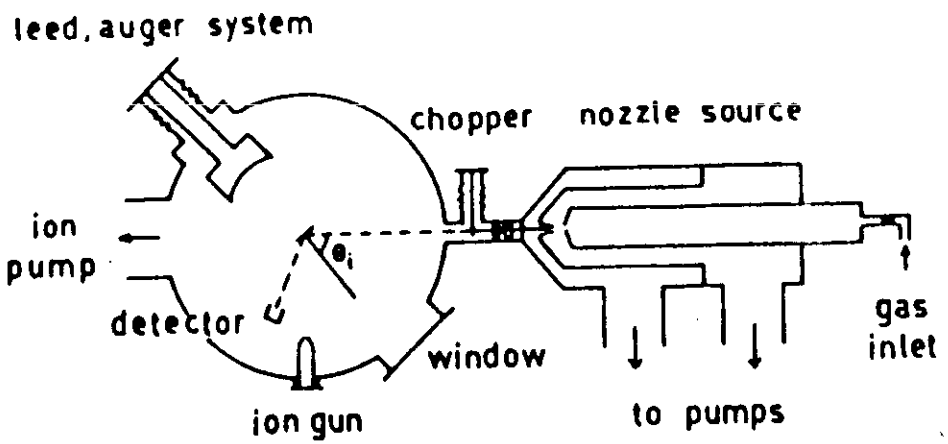

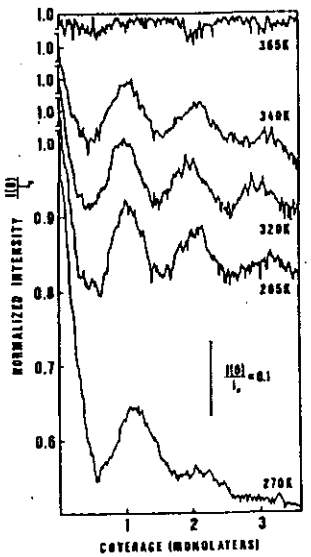

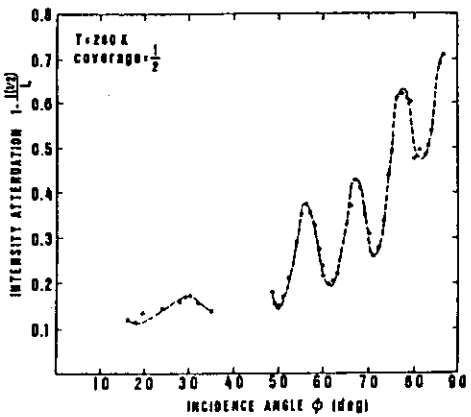

X-ray reflectivity from Ag(111)

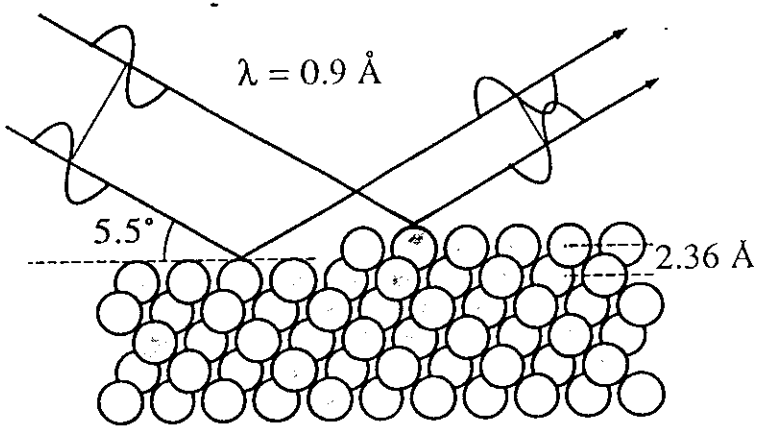

out-of-phase condition:
maximum sensitivity to islands

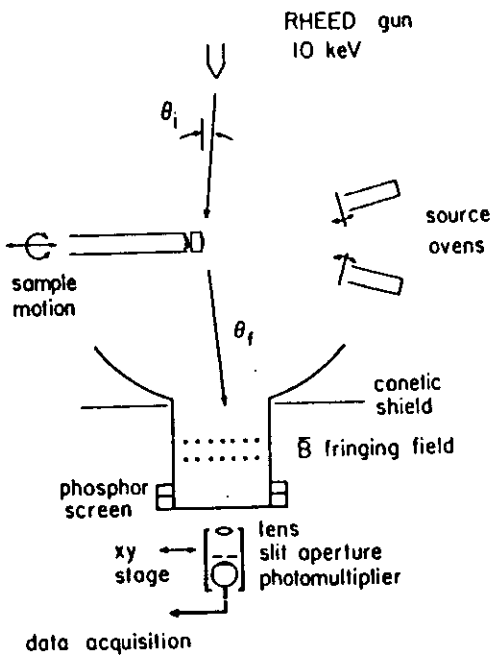
RHEED gun
10 keV
θ_i
source
ovens
sample
motion
θ_f
conetic
shield
$\vec{B}$ fringing field
phosphor
screen
lens
slit aperture
photomultiplier
xy
stage
data acquisition

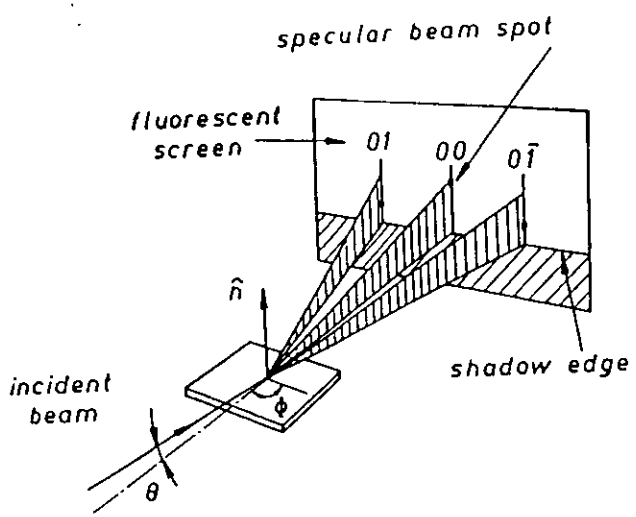
specular beam spot
fluorescent
screen
01
00
$0\bar{1}$
$\hat{n}$
incident
beam
shadow edge
ϕ
θ

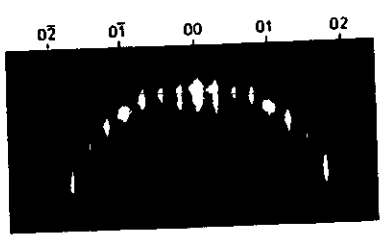
$0\bar{2}$
$0\bar{1}$
00
01
02

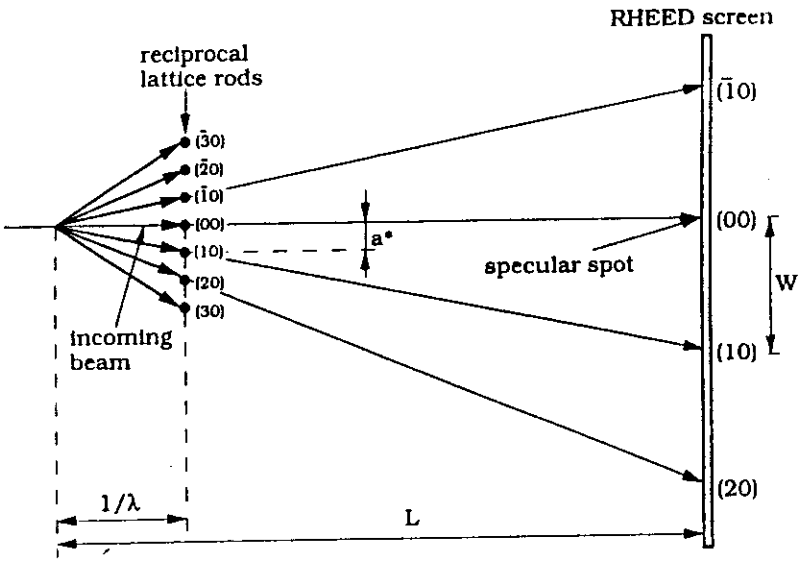

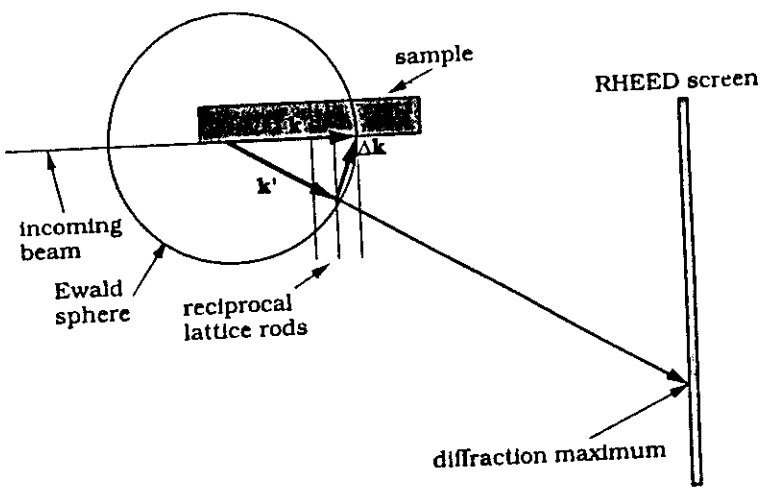

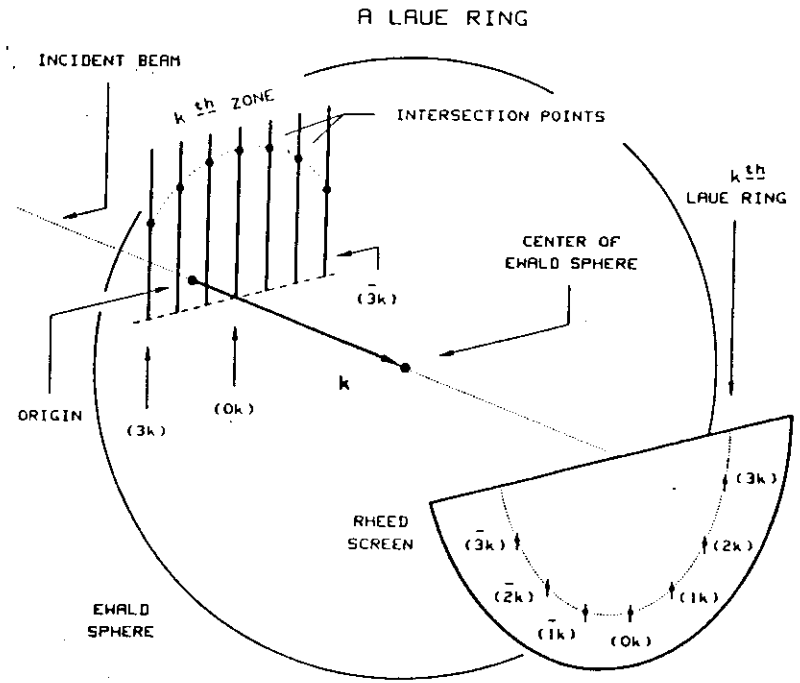

FIG. 6. A schematic diagram showing the formation of the k th Laue ring from the k th zone.

J.E. Mahan, K.M. Geib, G.Y. Robinson, and R.G. Long, JVST A 8, 3692 (1990).

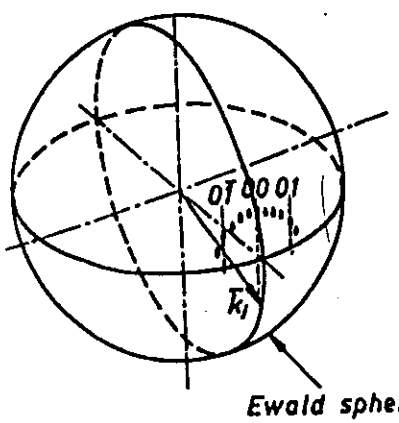

Fig. 4.10. Ewald sphere construction for the GaAs(001)-(2 × 4) reconstructed surface in [1̄10] azimuth, illustrating the arc of the short streaks corresponding to the intersection of the sphere with the 0Ī, 00, 01 and associated fractional-order rods. Higher-order Laue zones are omitted for clarity [4.14]

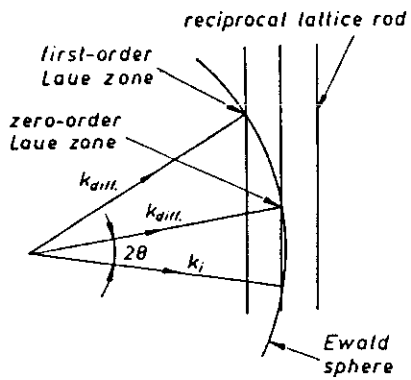

Fig. 4.7. Ewald sphere construction appropriate for a qualitative explanation of the formation of streaks in RHEED patterns. The wave vector k_i is very large compared with the interrod spacing [4.47]

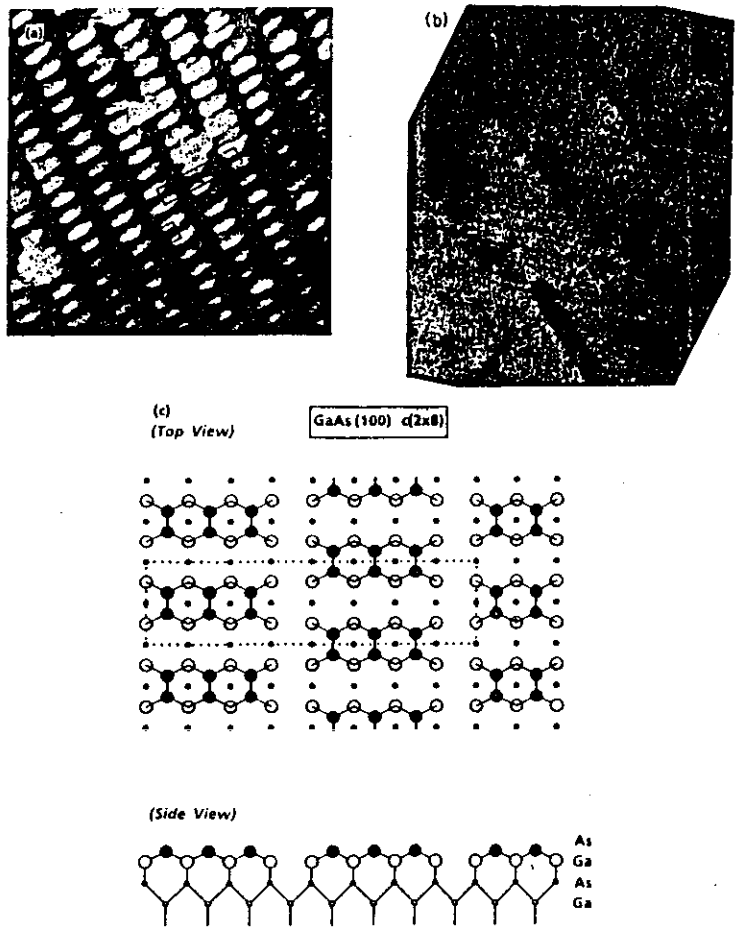

FIG. 2. (a) and (b) STM images of the GaAs(100)-(2×4) [or -c(2×8)] reconstruction at (a) lower and (b) higher resolution. Domains of 2×4 and c(2×8) can be seen to coexist. (c) Ball-and-stick model of the c(2×8) surface with three dimers per (2×4) subcell.

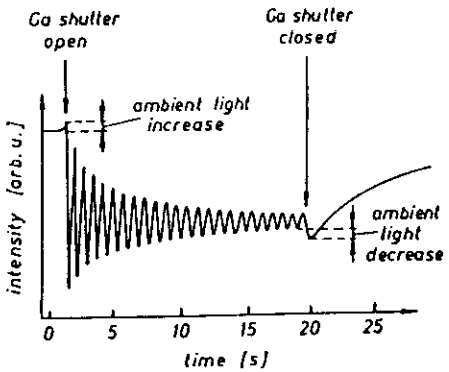

Fig. 1.8. Intensity oscillations of the specular beam in the RHEED pattern from a GaAs (001) 2 × 4 reconstructed surface [110] azimuth. The period exactly corresponds to the growth rate of a single Ga+As layer, and the amplitude gradually decreases. Note that the marked inflections at the beginning and end of growth result from ambient light changes as the shutters are opened and closed [1.91]

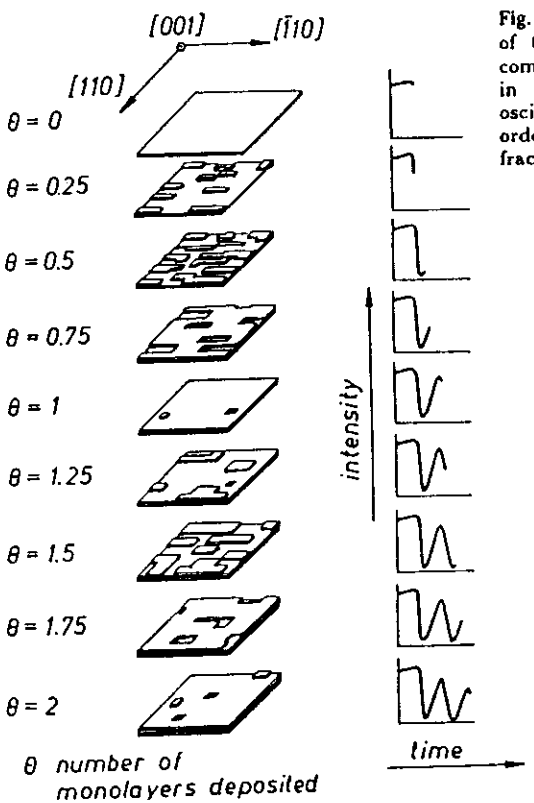

Fig. 1.9. Real space representation of the formation of the first two complete monolayers of GaAs(001) in relation to RHEED intensity oscillations, according to the first-order growth model. Here Θ is the fractional layer coverage [1.121]

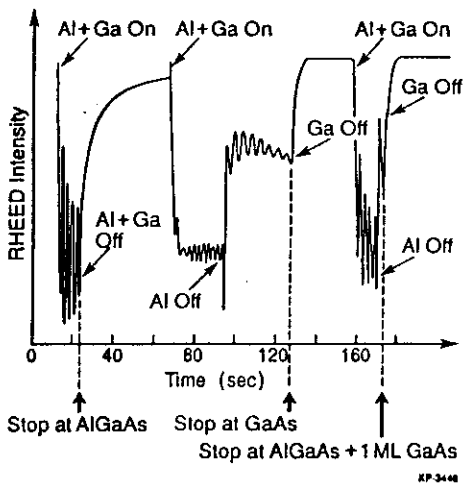

3. **2D multilayer growth:**

As adatom velocities decrease still further, clustering occurs more frequently, islands grow larger before they are incorporated into terraces, and several layers become exposed to the vapor flux simultaneously. However, *locally*, growth still remains two-dimensional on top of each terrace and island. Adatoms are still mostly incorporated at step edges (both intrinsic and extrinsic) and do not cross to other levels.

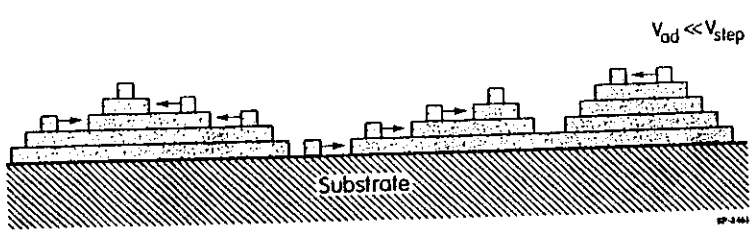

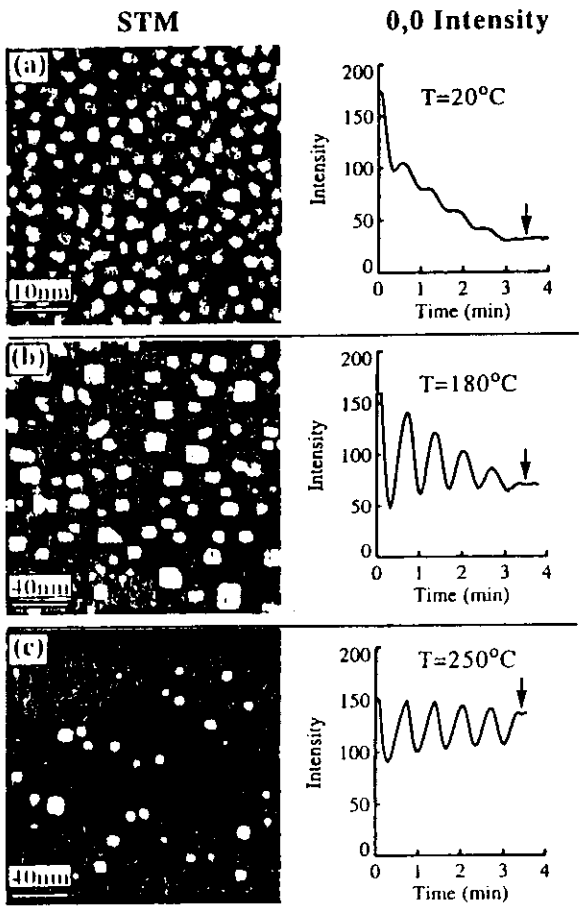

FIG. 2. STM and RHEED (0,0) beam intensity measurements of Fe on Fe(001) growth obtained on the same samples. All the films were grown for five RHEED oscillations, at which time the Fe flux was turned off, indicated by the arrows in the RHEED plots. The RHEED measurements were made with a 10 keV beam at the antiphase angle of incidence of 64 mrad. The intensity plots were obtained by integrating over the (0,0) diffraction spot by $\pm 0.05°$ in both directions. Sample temperatures during growth, rms roughness, and step densities are (a) 20°C, 0.116 nm, 1.74 nm^{-1}; (b) 180°C, 0.095 nm, 0.23 nm^{-1}; and (c) 250°C, 0.06 nm, 0.09 nm^{-1}. STM images are shown in a grey scale with black being the lowest height level. The major changes in grey level indicate a monatomic step. Image sizes are (a) 50×50 nm and (b), (c) 200×200 nm.

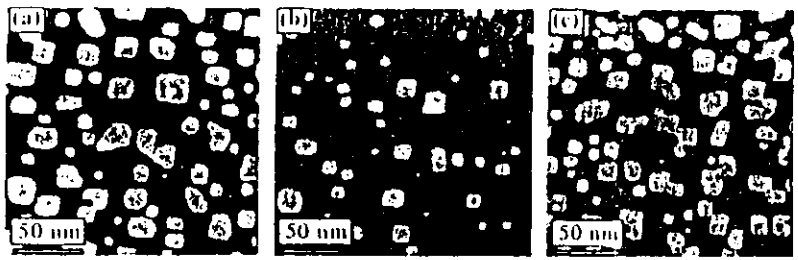

FIG. 3. (a)–(c) STM images after growing Fe on Fe(001) at a sample temperature 250 ± 20 °C for various numbers of RHEED oscillations: (a) 3.5, (b) 4.0, and (c) 4.5 oscillations. The corresponding coverages determined from the STM images are 3.32, 3.97, and 4.27 monolayers, respectively. Image sizes are all 200 × 200 nm.

Transition from Lay-by-layer to Multilayer Growth

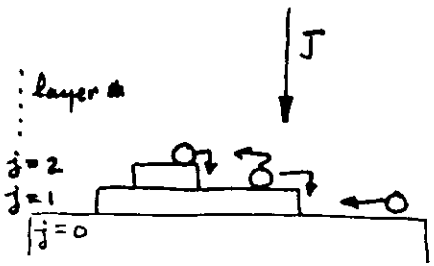

Interlayer mass transport is the crucial issue as is clear from a simple model developed by Cohen et. al. (Surf. Sci. 216 222 (1989).

$$\frac{d\theta_j}{dt} = \frac{J}{n_s}\left\{(\theta_{j-1}-\theta_j) - k_{j-1}^{-}(\theta_{j-1}-\theta_j) + k_j^{-}(\theta_j-\theta_{j+1})\right\}$$

Note that k_j^{+} is implicitly assumed to be unity.
Limits: (a) $k_j^{-} = 1$ when $\theta_j \neq 0$
(b) $k_j^{-} = 0$; i.e. a perfectly reflecting down step edge
In this case, accumulation on each terrace will be Poisson and $w = \sqrt{Jt}$

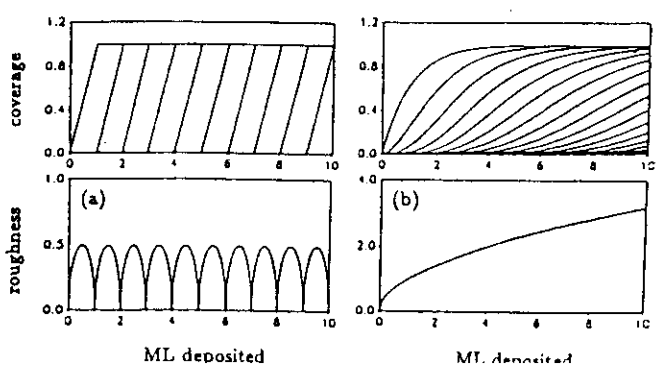

$w = \langle |h(x,t) - \langle h \rangle| \rangle^2$

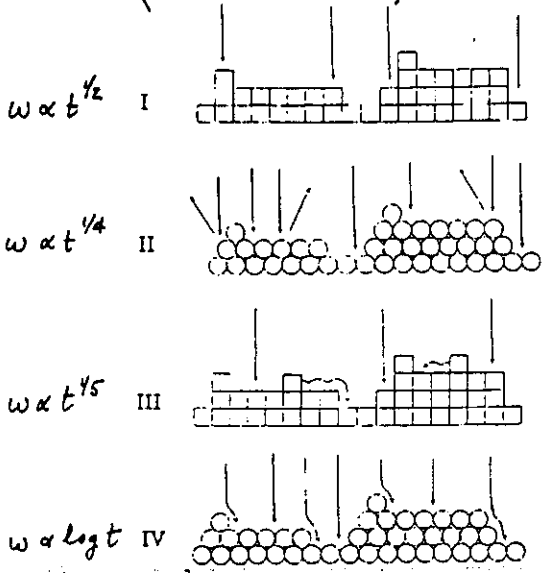

Fig. 6. Four simple lattice models of epitaxial growth.

I. "Hit and stick" model. ($S \equiv 1$).

II. Adatoms only stick if they land on a bridge site, otherwise scatter. (Introduces a crude site specific s).

III. Adatoms hit, stick, and diffuse to highest coordinated sites within a radius r. $E_B \equiv 0$.

IV. Slightly more sophisticated version of III. which favors downward hole-filling diffusion: "funnel down" mode

A. Zangwill, J. Cryst. Growth 163, 8 (1996).

Kinetic Monte Carlo Models (KMC)

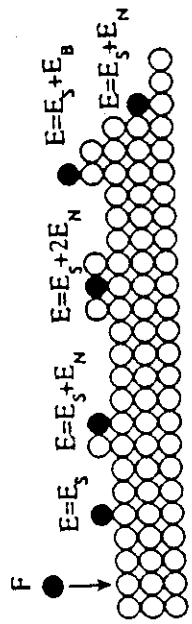

Illustration of kinetic roughening

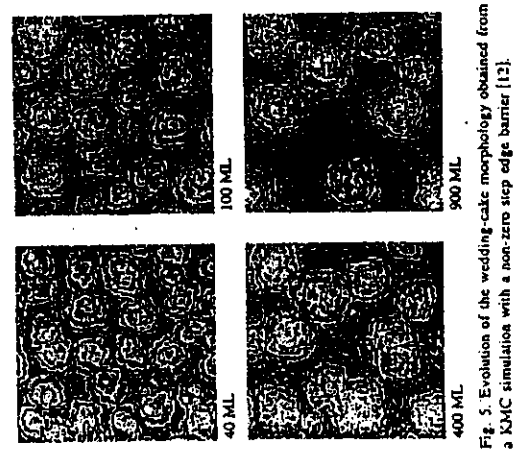

Fig. 5. Evolution of the wedding-cake morphology obtained from a KMC simulation with a non-zero step edge barrier [12].

P. Šmilauer and D.D. Vvedensky, Phys. Rev. B 48, 17603 (1993).

Fe/Fe(001)
$T_S = 20°C$

$\theta = 1$ ML

1000 x 1000 Å

200 x 200 Å

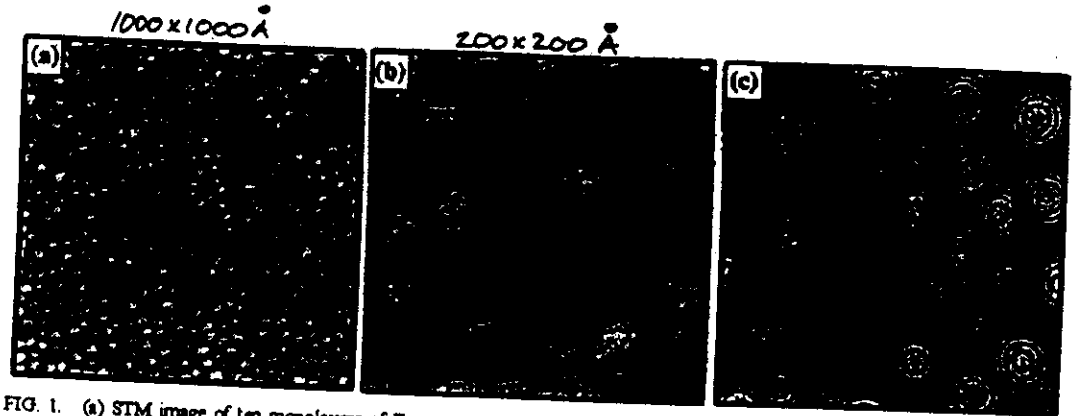

FIG. 1. (a) STM image of ten monolayers of Fe grown on an Fe whisker at 20 °C. The image is 100 × 100 nm, and the grey scale covers a range of 0.9 nm, where white indicates higher portions of the surface. Note the pattern formation of mounds. (b) Contour map of a smaller 20 × 20 nm region from the left bottom corner in (a). Solid lines denote equiheight contours with the heavy line at the mean height. (c) Contour plots of the calculated surface height during growth. The parameters for the current, Eq. (2), are $B = 1.0$, $\alpha = 2.0$, $\beta = 72.0$, and $\sigma = 20.0$. The numerical integrations are done on 64 × 64 lattices with $\Delta x = \Delta y = 1.0$. The initial conditions are randomly chosen for each site from a Gaussian distribution of width 0.01. The surface shown is at thickness $t = 56.23$.

J.A. Stroscio, D.T. Pierce, M.D. Stiles, A. Zangwill, L.M. Sander
PRL 75, 4246 (1995).

$\langle d \rangle \propto t^{0.16 \pm 0.04}$

$\langle d \rangle \propto t^{0.18 \pm 0.02}$

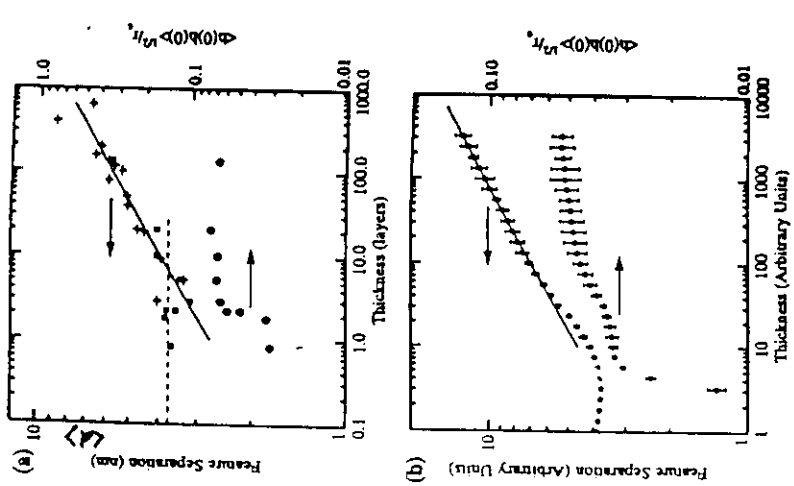

FIG. 3. (a) Feature separation and ratio of RMS height to feature separation versus film thickness. Left axis: feature separation L obtained from (squares) $2r_c$, where r_c is the first zero crossing of the height-height correlation function, and (diamonds) $4\pi/\Delta$, where Δ is the splitting of the RHEED diffraction peaks obtained from the profiles in the inset in Fig. 2. The solid line is the result of a least-squares fit to the STM and RHEED data points for thicknesses ≥ 20 monolayers yielding a slope of 0.16 ± 0.04. The dashed line is the island separation observed at 0.07 monolayer coverage [14]. Right axis: a measure of the angle that the mounds make with the surface plane estimated by taking the mound height as $\langle h(0)h(0)\rangle^{1/2}$ and the lateral extend of the mound as r_c. Fe evaporation rates were ~1.5 ML/min (open symbols) and ~30 ML/min (filled symbols). (b) Feature separation and ratio of RMS height to feature separation from numerical solution of the continuum equations. The feature separation and slope are derived from height-height correlation functions as in (a). Parameters of the integrations are as in Fig. 1(c). Each point

Use of Surfactants to Promote Homoepitaxy

Surfactant = a substance which lowers the surface tension, thereby increasing spreading and wetting properties.

Observations:
During metal MBE, some impurities present in sub-monolayer quantities promote homoepitaxial layer-by-layer growth.

Examples: Sb, In, Pt for Ag(111)
Sb for Ag(001)
In for Cu(001)
O_2 for Pt (111)

Proposed mechanisms:
* enhanced island nucleation rates
* alter average island shape to provide larger edge lengths (e.g., dendritic growth)
* decrease Ehrlich/Schwoebel barrier
*
*

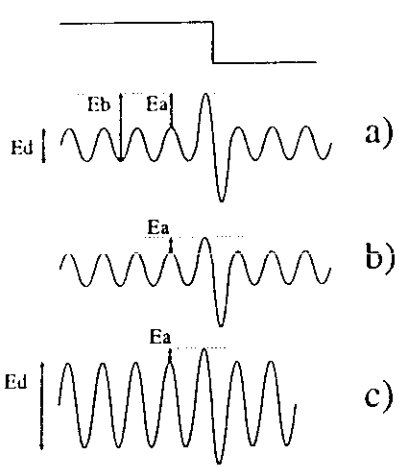

Figure 3.8: *Schematic surface potential at a step edge with a Schwoebel barrier. The Schwoebel barrier on the clean surface (a) can be decreased in two ways: (b) by a local decrease of the total barrier at the step or (c) by a global increase of the surface diffusion barrier. E_d denotes the surface diffusion barrier, E_b the total barrier at the edge, and E_a the additional (Schwoebel) barrier.*

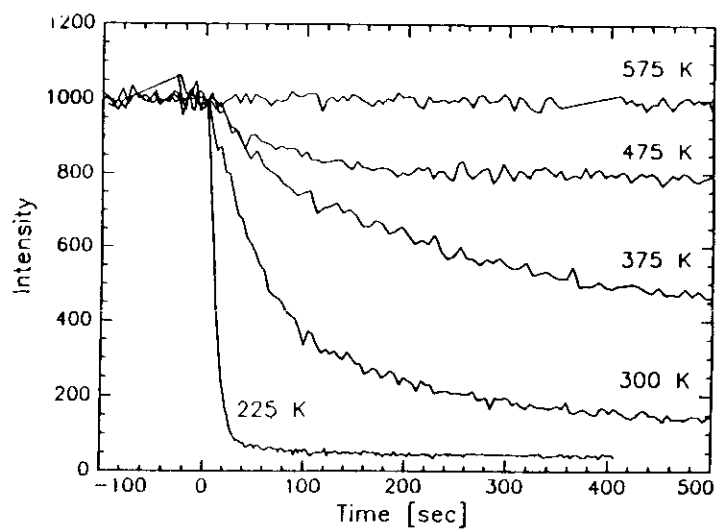

Figure 2.1: *The intensity of the (0 0 1.5) reflection during Ag deposition. Shown are a set of curves corresponding to different substrate temperatures. The curves are normalized to a starting signal of 1000.*

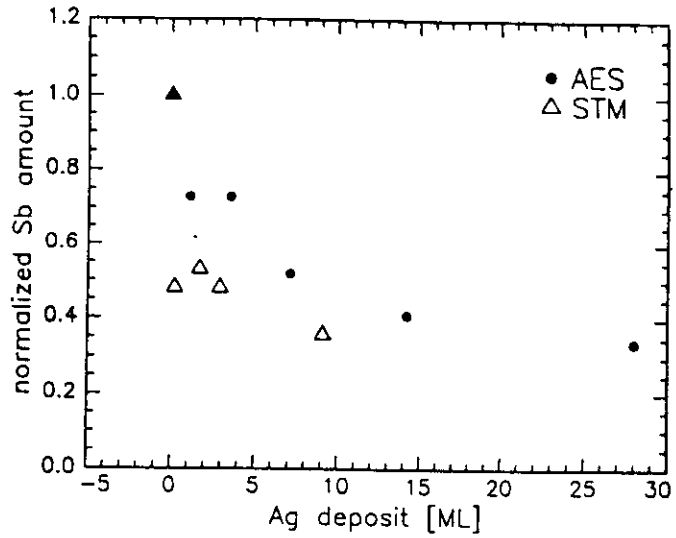

Figure 3.6: *The amount of Sb at the surface determined by AES (solid circles) and STM (triangles) as a function of the subsequently deposited Ag amount in ML. The Sb amount is normalized to the amount before Ag was added (0.5 ML for AES, 0.08 ML for STM).*

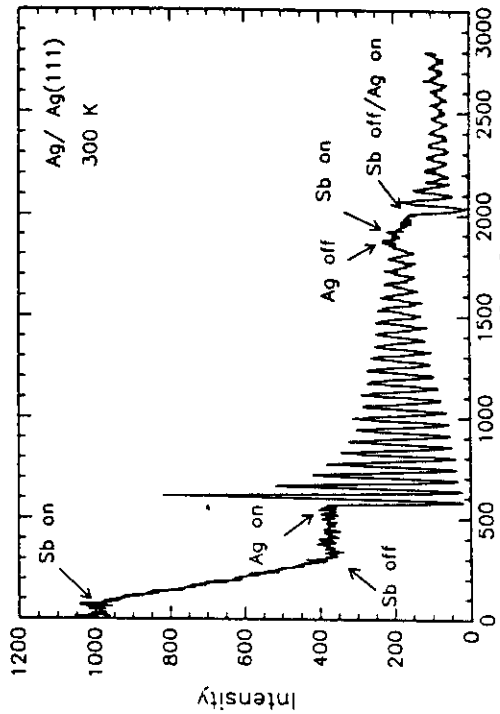

Figure 2.2: *The intensity of the* (0 0 1.5) *reflection during successive deposition of Sb (0.2 ML) and Ag at 300 K. At t = 0 the Ag deposition started. The intensity is normalized to a starting signal of 1000.*

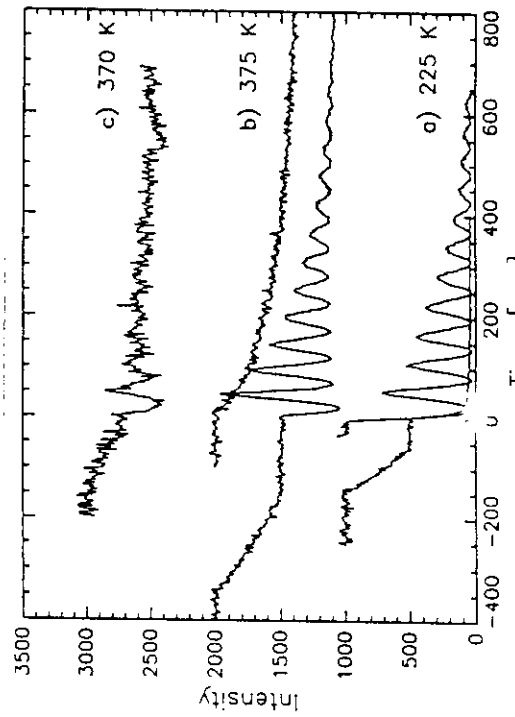

Figure 2.3: *The intensity of the* (0 0 1.5) *reflection after a fraction of a ML Sb was added at different substrate temperatures. (a) 225 K, 0.14 ML Sb, (b) 375 K, 0.15 ML Sb. For comparison the intensities without addition of Sb are plotted as well. In (c) the* (1 1 1.5) *reflection is shown: 370 K, ~ 06 ML Sb. The intensity is normalized to a starting signal of 1000, (b) and (c) have vertical offsets of 1000 and 2000 respectively.*

H.A. van der Vegt, H.M. Pinxteren, M. Lohmeir, E. Vleig, J.M.C. Thornton, PRL 68, 3335 '92

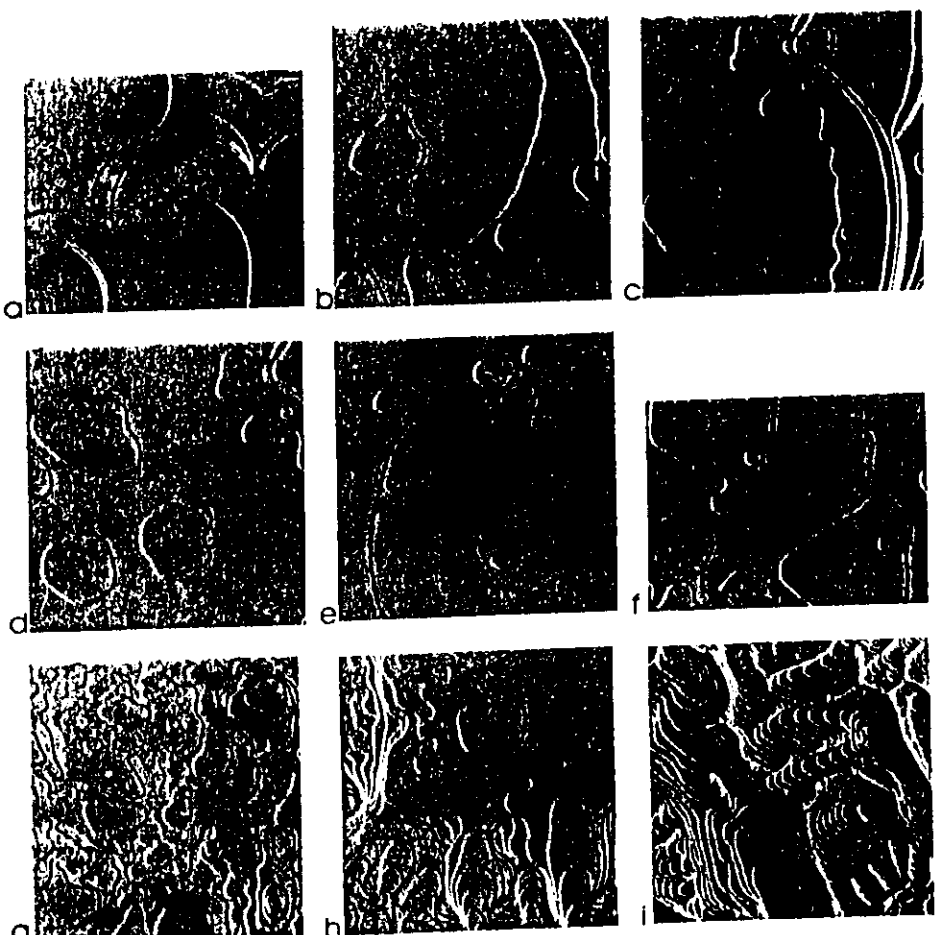

Figure 3.1: *Growth of Ag on a clean Ag(111) surface: a) Starting surface, size: 1400 nm × 1500 nm, b) After 0.12 ML Ag deposition, 700 nm × 740 nm, c) 0.24 ML Ag, 700 nm × 700 nm, d) 0.24 ML Ag, 750 nm × 750 nm, e) 0.24 ML Ag, 500 nm × 550 nm, f) 0.6 ML Ag, 850 nm × 550 nm, g) 2.7 ML Ag, 1100 nm × 1100 nm, h) 9.6 ML Ag, 750 nm × 650 nm, i) 25 ML Ag, 1100 nm × 800 nm.*

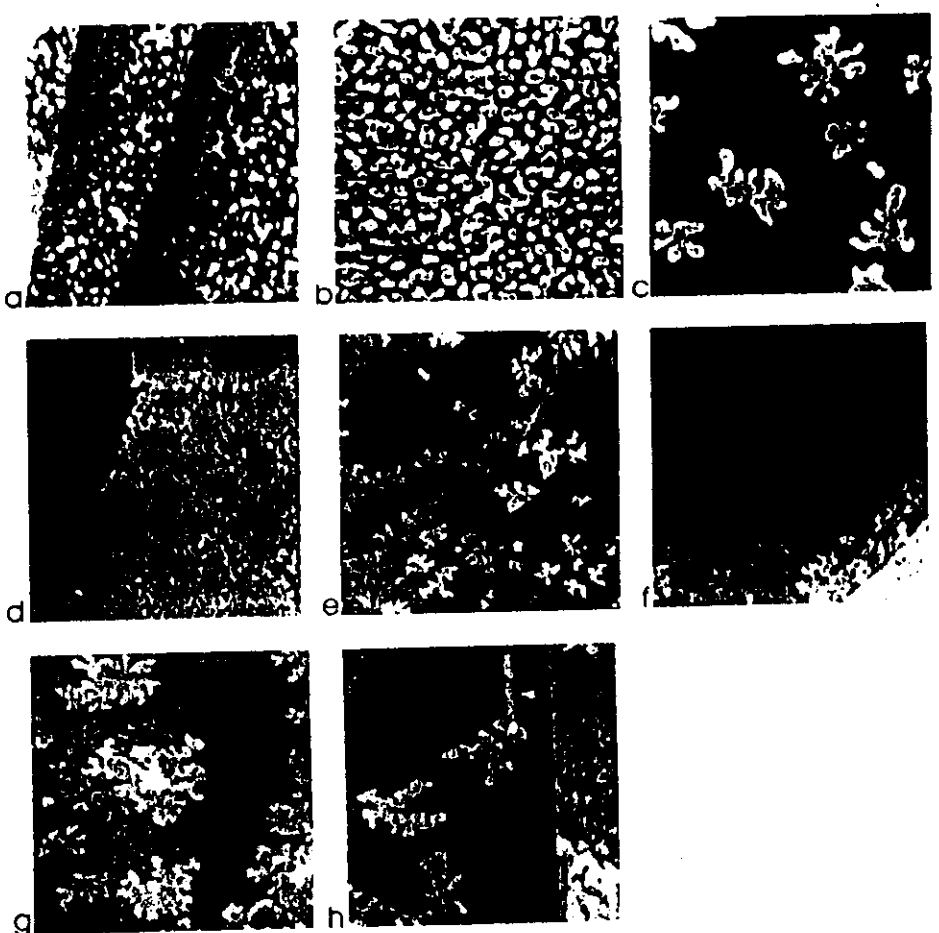

Figure 3.2: *Ag growth on an Sb precovered Ag(111) surface: a) 0.12 ML Sb, as deposited, 120 nm × 115 nm. The other images form a sequence of Ag growth after pre-deposition of 0.08 ML Sb: b) 0.5 ML Ag, 400 nm × 400 nm, c) 1.1 ML Ag, 450 nm × 450 nm, d) 1.7 ML Ag, 650 nm × 600 nm, e) 2.9 ML Ag, 600 nm × 550 nm, f) 4.3 ML Ag, 600 nm × 550 nm, g) 9.1 ML Ag, 400 nm × 400 nm, h) 11 ML Ag, 350 nm × 350 nm.*

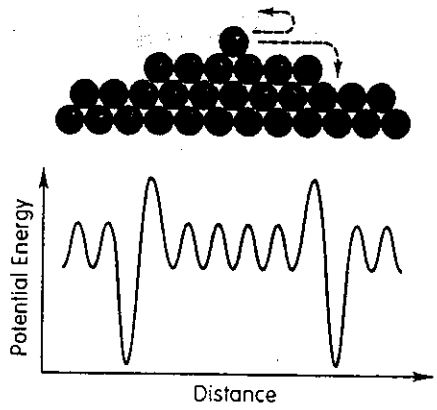

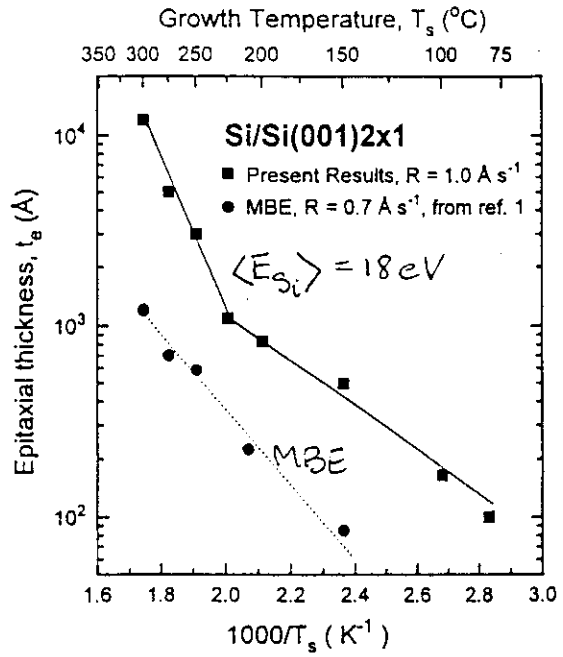

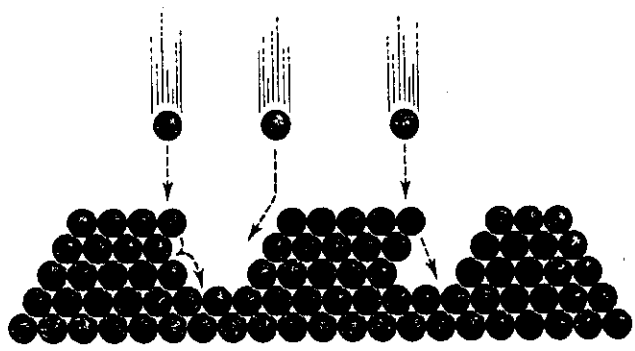

N-E. Lee, G. Tomasch, J.E. Greene, Appl. Phys. Lett. 65, 3236 (1994).

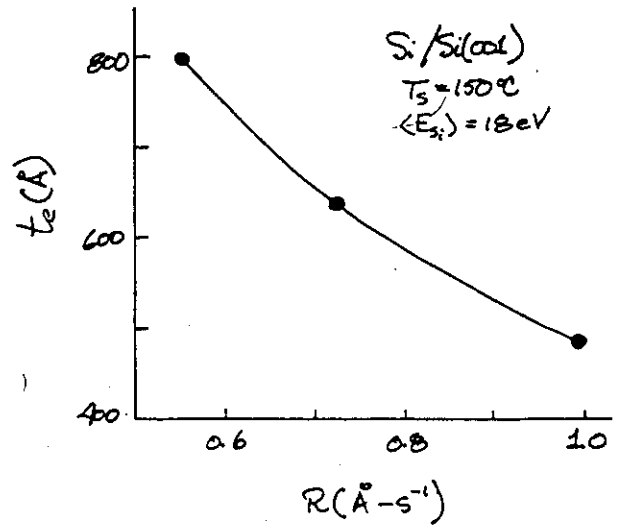

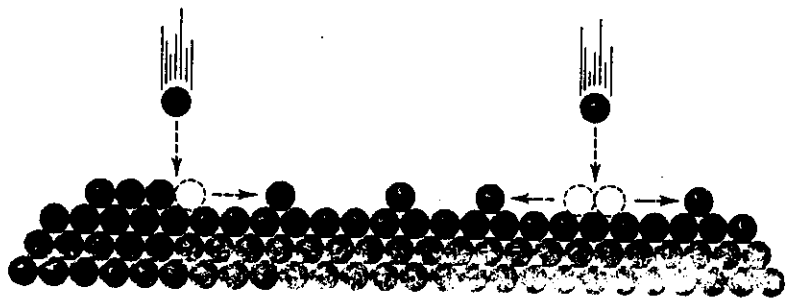

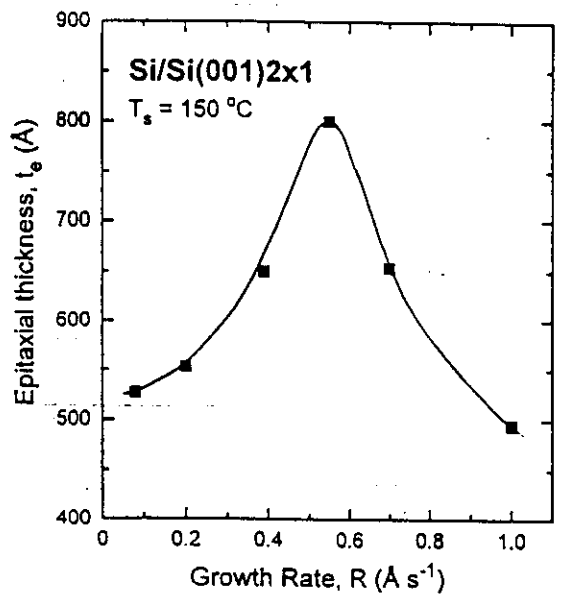

N-E Lee, G. Xue, J. E. Greene, J. Appl. Phys. 80, 812 (1996).